

Physical–mechanical consolidation and protection of Miocenic limestone used on Mediterranean historical monuments: the case study of *Pietra Cantone* (southern Sardinia, Italy)

Stefano Columbu¹ · Carla Lisci¹ · Fabio Sitzia¹ · Giampaolo Buccellato²

Received: 15 April 2016 / Accepted: 31 January 2017
© Springer-Verlag Berlin Heidelberg 2017

Abstract The present work aims to study the consolidating and protective chemical treatments of the *Pietra Cantone*, a Miocenic (lower Tortonian) limestone widely used in important monuments and historical buildings of Cagliari (southern Sardinia, Italy). Similar limestones of the same geological period have also been used in several important monuments of Mediterranean area, i.e., Malta and Gozo Islands, Matera (central Basilicata, Italy), Lecce (southern Puglia, Italy) and Balearic Islands (Spain). The *Pietra Cantone* limestone shows problems of chemical–physical decay, due to their petrophysical and compositional characteristics: high porosity (on average 28–36 vol%), low cemented muddy-carbonate matrix, presence of phyllosilicates and sindepositional sea salts (<3%). So, after placed in the monument, this stone is easily alterable by weathering chemical processes (e.g., carbonate dissolution and sulfation) and also by cyclic mechanisms of crystallization/solubilization of salts and hydration/dehydration of hygroscopic phases of the clay component. To define the mineralogical-petrographic features (composition, texture) of limestone, the clay and salt crystalline phases, the optical microscope in polarized light and diffraction analysis were used. To define the petrophysical characteristics (i.e., shape and size distribution of porosity, surface area

(SBET), matrix microstructures, rock composition) and interactions of chemical treatments with rock, SEM–EDS analysis and N₂ porosimetry with BET and BJH methods were used. To evaluate the efficacy of Na/K-silicates, ethyl silicate consolidants and protective nano-molecular silane monomer water repellent, the mechanical strengths (uniaxial compressive strength, point load and flexural resistance), water/helium open porosity, water absorption and vapour permeability data determined before and after the chemical treatments of the *Pietra Cantone* samples from monument were compared.

Keywords Limestone alteration · Porosity · Mechanical strength · Vapour permeability · Chemical treatment · Cultural heritage conservation

Introduction

Sedimentary rocks (e.g., limestone, sandstone, etc.), particularly those of carbonate type, are widely used in the construction of historical buildings in Sardinia island as well as in many Italian monuments or other Mediterranean countries. This is generally due to their more easy availability in the territory and especially to their better workability compared to silicate igneous or metamorphic rocks (Antonelli et al. 2014a, b; Bertorino et al. 2002; Columbu et al. 2014a). Some kinds of volcanic rocks only (i.e., pyroclastites with dacitic or rhyolitic composition) characterized by low-medium welding, due to their excellent workability (similar to those of carbonate rocks), are also widely used as construction materials in historical times, from Punic–Roman to Romanesque times (Columbu et al. 2011, 2013, 2014b, 2015a, 2015b, 2016a; Columbu 2017; Columbu and Garau 2017; Columbu and Sitzia 2016;

This article is part of a Topical Collection in Environmental Earth Sciences on “Geomaterials used as construction raw materials and their environmental interactions” guest edited by Richard Přikryl, Ákos Török, Magdalini Theodoridou, and Miguel Gomez-Heras.

✉ Stefano Columbu
columbu@unica.it

¹ Dipartimento di Scienze Chimiche e Geologiche, Università degli Studi di Cagliari, Via Trentino 51, 09127 Cagliari, Italy

² Produzioni Freius Chimici, Buccellato S.r.l., Sestu, CA, Italy

Columbu and Verdiani 2012, 2014; Coroneo and Columbu 2010; Melis and Columbu 2000; Macciotta et al. 2001; Miriello et al. 2015; Verdiani and Columbu 2010).

The Miocene limestones outcropping in the Cagliari city area (southern Sardinia, Italy, Fig. 1) are frequently used in the civil and historical architecture. These limestones belong to the sedimentary and volcanic stratigraphic sequence widely outcropping inland from Cagliari within the “Fossa Sarda” graben (Vardabasso 1962), a complex geological-tectonic context of Sardinia (Advokaat et al. 2014a, b; Casula et al. 2001; Cherchi and Tremolieres 1984). The Miocene serie of Cagliari area mainly consists (bottom in the stratigraphic sequence) of the following three facies: clays (“Argille del Fangario”), sandstones (“Arenarie di Pirri”), marly limestones (*Pietra Cantone*), biocalcarenes (“Tramezzario”) and the biohermal limestones (“Pietra forte”) (Barroccu 2010; AA.VV. 2005; Barroccu et al. 1981; Cherchi 1971; Gandolfi and Porcu 1967; Pecorini and Pomesano Cherchi 1969). The “Pietra forte” is a compact limestone and physical–mechanical resistant, and therefore difficult to work.

On the other hand, the *Pietra Cantone* stone is a marly limestone characterized by low cementing degree and high porosity (28–36 vol%). It has a CaCO₃ content generally assessed on the order of 75–80%, but can vary between 64 and 89% (Barroccu et al. 1981) depending on the different areas of Cagliari and on the depth of sedimentation. The *Pietra Cantone* generally shows a variable clay component (ranging from 10 to 30%) within the geological formation. Given the easy workability and the wide availability in the territory around Cagliari, this limestone has been widely used to the historical buildings (Fig. 2) of all periods from Nuragic, to Phoenician–Punic, Roman and medieval (Columbu et al. 2015a; Columbu and Pirinu 2016; Columbu and Verdiani 2014). It has a remarkable ease in processing, and for that reason, it is named “cantone” which means ashlar (Lovisato 1901). When this stone is used on monuments in the presence of humidity or circulating aqueous solutions, it shows frequently decay problems (Columbu et al. 2016b), when it is not protected by lime plaster.

The chemical–physical decay is also due to hygroscopic volume variations of clay minerals and sea salts, which are present in the rock and that make the limestone easily degradable with a decrease in mechanical strength. When the limestone is used in the structural elements of monuments (e.g., ashlar in the wall, column and jambs; Figure 2), the decay can lead to the formation of serious static-structural criticality in the buildings, as a strong retreat of vertical profile of the facade or detachment of the material portions from the decorative working parts, due to exfoliation and flaking processes (Fig. 3a–f).

The same alteration processes are also present in other limestones which are similar to the used *Pietra Cantone*,

Fig. 1 Geological map of Cagliari area. Geological thematism according to AA.VV. 2007 (P.U.C. “Urban development plan” of Cagliari, 1997). Scale mapping 1:25.000. Original legend derives partly from hydrogeological map of Cagliari 1:10.000 of Pala and Siriu 1997, modified

e.g., in the baroque architecture of Lecce (a Miocenic calcarenitic stone known as “Pietra di Lecce”; Rodolico 1953; Zezza et al. 1990) and Noto in Sicily (Alessandrini et al. 1992; Rodolico 1953), in Pisan medieval architecture (e.g., Macigno sandstone, Monti d’Oltre Serchio limestone; Lezzerini et al. 2016), in Majorca in the Balearic Islands (Rodolico 1953), in well-known megalithic temple complex (4th–3rd millennium BC) on the Malta and Gozo islands (“globigerina limestone”, Vannucci et al. 1994), etc.

To prevent such decay of carbonate rocks which are used in the monuments, efforts are numerous in regard to their water protection and surface consolidation, from ancient time (Giamello et al. 2016) to laboratory experimentation. These chemical treatments differ both in typology of products and in application methods (e.g., Camaiti and Columbu 2016). However, due to the different chemical–physical–petrographical characteristics of these lithologies, microclimatic conditions and alteration degree of the artefacts, the conservative techniques must be adapted to each case individually. Silicon-based polymeric materials applied as monomers (e.g., ethyl silicate), or as oligomers or polymers or nano-dispersions (e.g., nano-silica), vinyl polymers (e.g., acrylic resins, fluoro-elastomers) or inorganic products, such as nano-limes and oxalates, are very common.

In the scientific literature, several authors have dealt in various ways from a geological, geomechanical and engineering point of view with the limestones of the Cagliari area (Barroccu et al. 1981; Carmignani and Sassi 1991) or similar lithologies. Through non-destructive analytical methods (seismic surveys, ultrasonic and thermographic methods; e.g., Christaras et al. 2015; Concu and Fais 2003; Concu et al. 2003a, b; Concu and Valdes 2007; Diana and Fais 2011; Fais et al. 2015) and physical–mechanical tests in laboratory and in situ (Barroccu et al. 1981), some authors (Colback and Wiid 1965) have studied some physical parameters of these rocks (mechanical strength, porosity, density, often calculated by indirect way). Other authors have studied the relationships between the microstructural properties (composition, grain and pore size), especially how the fluids flow through the network of porous media (Carman 1937; Francis and Dullien 1975) and macroscopic performance of the stone (Price 1996). Atzeni et al. (1991, 2006) have quantitatively explored the mechanisms of water-induced microstructural weakening in a porous limestone under water “static” presence and

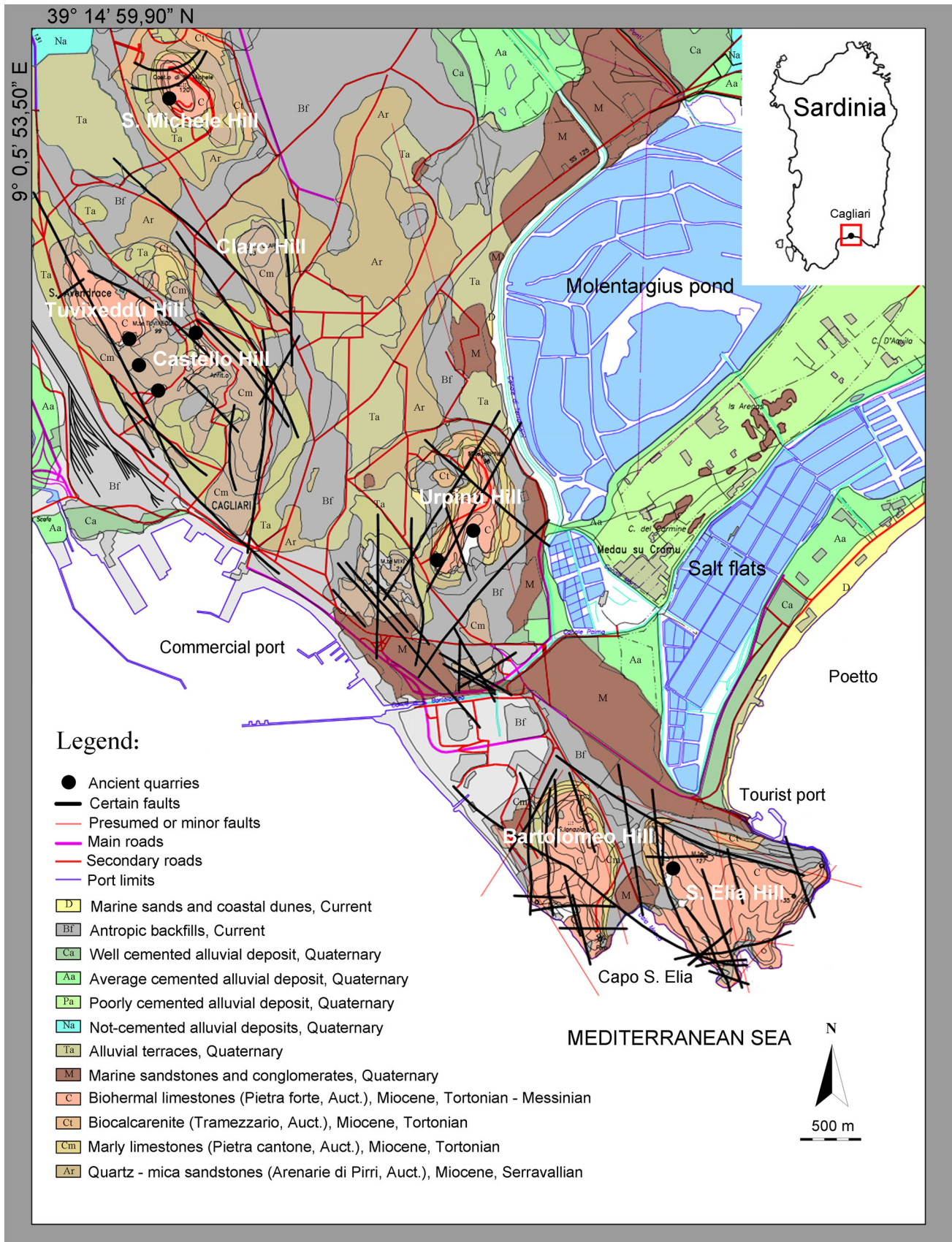




Fig. 2 **a** Town Hall of Cagliari. The *Pietra Forte* building stands on a Sardinian granitic plinth (1899–1915); **b** facade of the *San Saturnino* Basilica built in 304 AD with the *Pietra Cantone* limestone. The church was founded originally as a *martyrium* in honour of the Saint *Saturnino* Patron of Cagliari; **c** Façade of *Nostra Signora di Bonaria*, Sanctuary dated 1704 built with the *Pietra Forte*; **d** *San Michele* church (1664–1712 AD). The façade is built with

Pietra Forte limestone and the perimeter wall outside partly in *Pietra Cantone* limestone; **e** *Santa Croce* Basilica built in 1661 AD entirely with *Pietra Cantone*. Alteration phenomena are noticed such alveolation; **f** *Cattedrale di Santa Maria di Castello* (1669–1674). The facade is built entirely with *Pietra Forte*. The interior is characterized by fine Greek marble and mosaics adorn the walls

flow conditions using the *Pietra Cantone* of Cagliari as experimental model. But only few more targeted investigations were made in the laboratory to understand how the physical–mechanical properties influence the behaviour of this limestone taken directly from the monuments with respect to conservation treatments of consolidation and protection. On the basis of technical-practice experience gained by Buccellato-Freius company during several years of restoration activities on monuments made among other materials out of limestones, including the *Pietra Cantone* (e.g., Torre di San Pancrazio, City Hall and Cathedral of

Cagliari, Ghetto of Jewish, Santa Croce church, Tobacco Factory, St. Ambrogio church of Monserrato, Porto Flavia in Masua, etc.), Na/K-silicates and ethyl silicate give all in these monuments the most satisfactory results. Given the high porosity of these limestones, the optimal application in situ is the injection of consolidating products under controlled pressure through coring in masonry, which consequently includes the consolidation of the mortars too. The number and spacing of the carrots is dependent on the alteration degree of the stone and the deep of material portion affected by the decay.

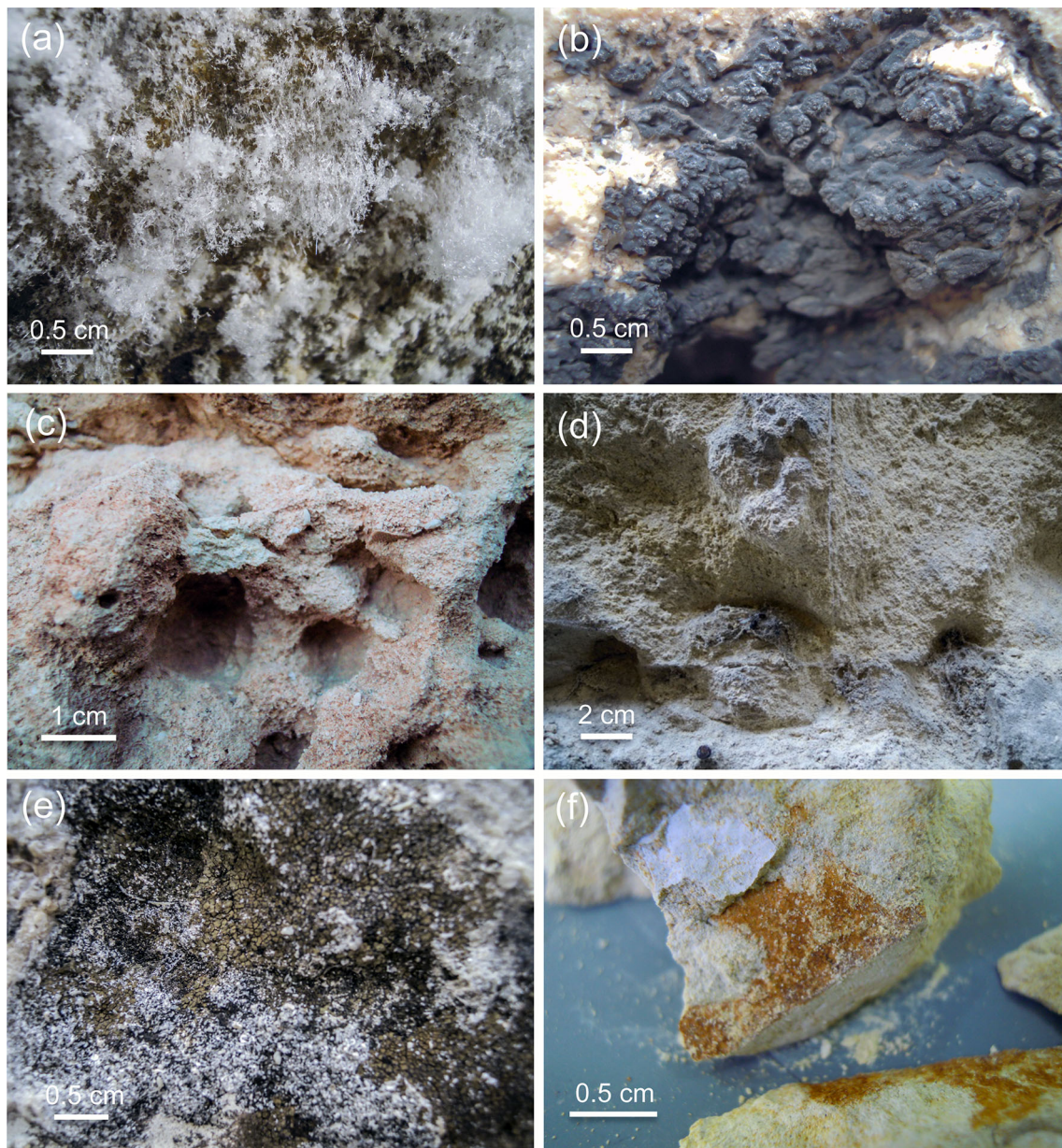


Fig. 3 Typical alteration forms of limestones from Cagliari area: **a** efflorescence in the inner wall of *San Saturnino Basilica*; **b** black crusts with gypsum and black carbon particles in the *San Pancrazio tower*; **c** strong alveolation of the outsider wall of *San Michele church* built in *Pietra Cantone*; **d** alveolation and pulverization with

advanced physical decay of *Pietra Cantone* with ashlar retreat of *Santa Croce Basilica* facade; **e** examples of biodegradation of limestone due to the proliferation of lichens on a vertical wall in areas where humidity and dripping processes are concentrated; **f** interbedding clayish layer in MSA samples

However, in some monuments with high historical-cultural relevance, it is not possible to operate the coring due to limitations imposed by the local Superintendence of Cultural Heritage. In these cases, minimally invasive procedures need to be used for the application of the products, i.e., brushing or spraying in two or more coats spaced 10 h apart.

As regards the protective water repellent, it was noticed that the silane monomer is more suitable due to its high penetration (with small molecule diameter) and good

chemical–physical compatibility with rock (Croveri et al. 2004; Escalante et al. 2000). This product is spread through brushing or spraying up to rejection by the stone in two or more coats, wet on wet, close after each other. In the case of less porous rocks (<20 vol%), the product has to be given with gradually higher concentrations (according to Buccellato–Freius experience).

The present work aims to evaluate in the laboratory the efficacy of Na/K-silicates (called CM), ethyl silicate (called FB) consolidants and a protective water repellent

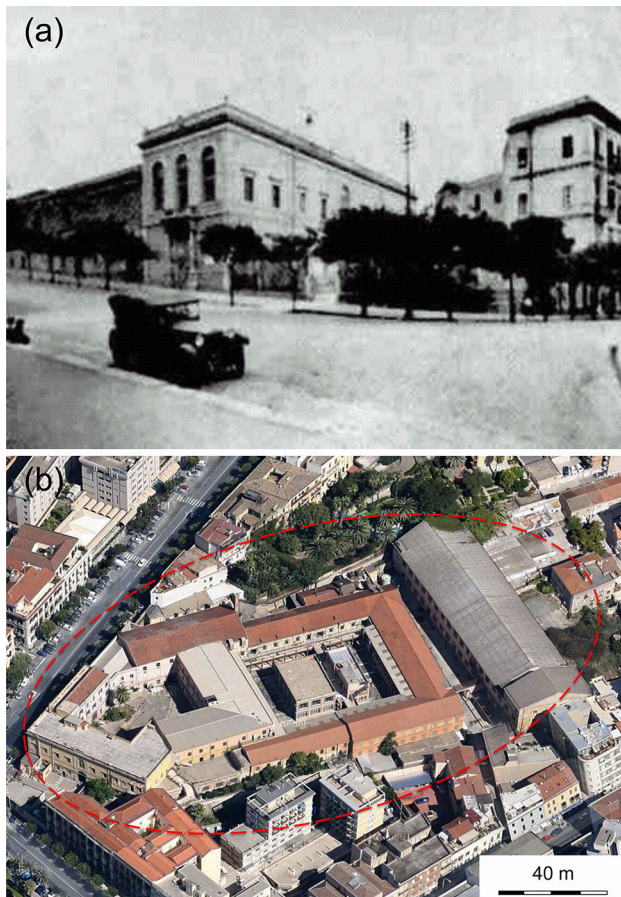


Fig. 4 **a** Historical image of ancient Tobacco Factory of Cagliari (eighteenth century) located in Viale Regina Margherita (Cagliari). Source www.aladinpensiero.it/wp-content/uploads/2014/09/MANI_FATTURATABACCHI-CA-novecento.jpg; **b** Recent external view of ex Tobacco Factory of Cagliari, now with a new destination of “Creativity Factory” (not yet definitively open to the public). Coordinates: 39°12′46.76″N–9°07′00.1″E. Source copyright: www.gosur.com/satellite: street map modified

based on nano-molecular silane monomer (called NG) on three *Pietra Cantone* samples belonging to the masonry walls of an ancient building (fourteenth century AD) that has been modified over time to become in the eighteenth century an important tobacco factory of Italian “Monopolio di Stato” (Fig. 4a, b).

To evaluate the performance of the selected chemicals, a comparison of mechanical and physical properties (i.e., point load, compressive and flexural strengths; water absorption; porosity; gas permeability) determined before and after the chemical treatment of the limestone samples has been done. Moreover, the physical properties, in addition to being useful for a basic characterization of a rock (Columbu et al. 2015c), allow to study the alteration processes and to evaluate the decay state of the limestone.

The three *Pietra Cantone* samples taken from the monument (signed with MSA, MSB, MSC) were treated with impregnation for gradual immersion (for consolidant)

and brushing (for water repellent). The immersion mode allows an optimal distribution of the product inside the stone matrix with widespread and uniform penetration in the outer portion. The immersion method also allows to dose the correct amount of product to be applied in the monument stone to obtain an optimum result.

Materials and methods

Sampling and geomaterials

The sample material was collected from the masonry-walls of the tobacco factory during its restoration that occurred a few years ago. Three big fragments (MSA, MSB, MSC) of three ashlar of *Pietra Cantone* limestone (Fig. 5) were collected, compatibly with the limits imposed by the local Superintendence of Cultural Heritage. The sampling was done with minimally invasive methods, trying not to deface the monument, not to affect the building structure and to preserve its original characteristics.

The samples were taken at different heights in the inner wall of tobacco factory masonry.

In laboratory, the following specimens were cut from each sample: cubic specimens with size $\sim 15 \times 15 \times 15$ mm on which to determine the physical properties (real and bulk density, porosity, water absorption); prismatic

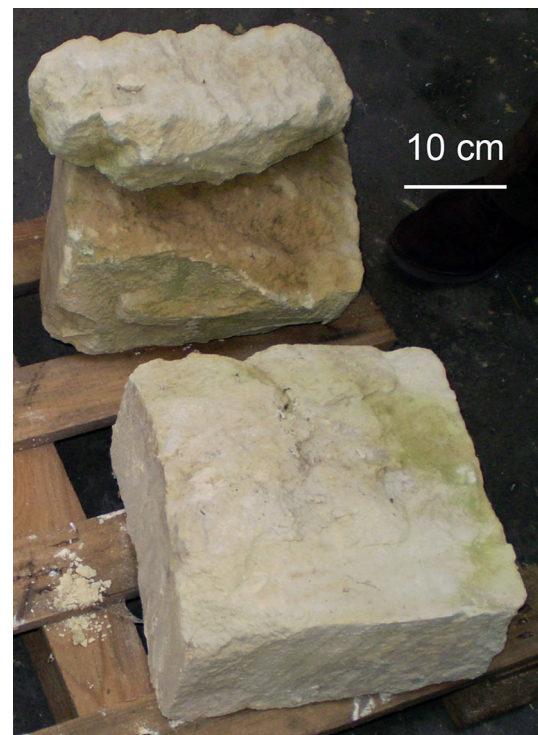


Fig. 5 Some samples of *Pietra Cantone* ashlar taken from Tobacco Factory monument of Cagliari

specimens with $\sim 50 \times 50 \times 10$ mm for vapour permeability; cubic specimens with $\sim 50 \times 50 \times 50$ mm for uniaxial compressive tests; prismatic specimens with $12 \times 50 \times 20$ mm for flexural tests; thin sections of about 30 μm thickness for the microscopic analysis; and powdered samples for XRD analysis.

Petrographic and physical methods

Petrographic determinations of mineralogical composition were carried out by optical polarized microscopy (OM) on polished thin sections using a Leitz Wetzlar microscope.

For the qualitative mineralogical characterization of the crystalline phases in powder samples, X-ray diffraction analysis (XRPD) was used an experimental package Geigerflex Rigaku D/MAX-B/C series, equipped with a monochromator system, using the $\text{CuK}\alpha$ ray tube radiation at 30 kV and 30 mA, Ni filter, scan 4–60 or 3–90°2 θ , sampling pitch of 0.01°2 θ .

To deepen knowledge on the composition and microstructural aspects of the *Pietra Cantone*, SEM analysis of broken and sawn samples was made. SEM microscopy investigation and microphotographs were performed with a Zeiss Evo LS 15 equipped with a LaB_6 filament as electron source.

Inner surface area and pore volume of the adsorbents were measured from nitrogen sorption isotherms at 77 K on a Micrometrics ASAP 2020 sorption analyser. Prior to any measurement, samples were outgassed at 150 °C for 12 h under vacuum, to remove any gases or vapours that may have become physically adsorbed onto the adsorbent surface. A thermic treatment at $T > 150$ °C of clay minerals allows the removal of the physical adsorption water and part of the hydration water. According to Che et al. (2011), the thermogravimetric analysis show that the dehydration processes indicated that most of their interlayer H_2O molecules were lost by 200 °C. The dehydroxylation of clay minerals starts at $T > 400$ °C: the kaolinite starts at 463.77 °C (Bontle and Nadiye-Tabbiruka 2007); the montmorillinte group minerals began to lose their structural OH groups gradually from 600 to 700 °C. XRD data of clay samples treated at 300 °C showed that they retained their original crystallographic structure (Che et al. 2011).

Surface area (SBET) was determined using the Brunauer–Emmet–Teller (BET) equation according to consistency criteria (Walton and Snurr 2007), and the total pore volume (V total) was calculated from amount of N_2 adsorbed at relative pressure of $P/P_0 = 0.99$. Mesopore size distribution was derived from the Barrett–Joyner–Halenda (BJH) method (Barrett et al. 1951).

The physical tests to determine the porosity, water absorption by immersion and density were determined according to the following methods. The specimens were

dried at 105 ± 5 °C, and the dry solid mass (m_D) was determined. The solid phases volume (V_S) of powdered rock specimens (on 5–8 g and with particle size less than 0.063 mm) and the real volume (V_R) with:

$$V_R = V_S + V_C \tag{1}$$

(where V_C is the volume of pores closed to helium of the specimens) were determined by helium Ultrapycnometer 1000 (Quantachrome Instruments). Then, the wet solid mass (m_W) of the samples was determined until constant weight. Through a hydrostatic analytical balance, the bulk volume (V_B) with

$$V_B = V_S + V_O + V_C \tag{2}$$

where

$$V_O = (V_B - V_R) \tag{3}$$

is the volume of open pores to helium is calculated as:

$$V_B = \left[\frac{(m_W - m_{HY})}{\rho_{WT\ 25^\circ\text{C}}} \right] \cdot 100 \tag{4}$$

where m_{HY} is the hydrostatic mass of the wet specimen and $\rho_{WT\ 25^\circ\text{C}}$ is the water density at a temperature of 25 °C.

Total porosity (Φ_T), open porosity to water and helium ($\Phi_{O\text{H}_2\text{O}}$; $\Phi_{O\text{He}}$, respectively), closed porosity to water and helium ($\Phi_{C\text{H}_2\text{O}}$; $\Phi_{C\text{He}}$), bulk density (ρ_B), real density (ρ_R) and solid density (ρ_S) were computed as:

$$\Phi_T = \left[\frac{(V_B - V_S)}{V_B} \right] \cdot 100 \tag{5}$$

$$\Phi_{O\text{H}_2\text{O}} = \left\{ \frac{\left[\frac{(m_W - m_D)}{\rho_{WTx}} \right]}{V_B} \right\} \cdot 100 \tag{6}$$

$$\Phi_{O\text{He}} = \left[\frac{(V_B - V_R)}{V_B} \right] \cdot 100 \tag{7}$$

$$\Phi_{C\text{H}_2\text{O}} = \Phi_T - \Phi_{O\text{H}_2\text{O}} \tag{8}$$

$$\Phi_{C\text{He}} = \Phi_T - \Phi_{O\text{He}} \tag{9}$$

$$\rho_S = \frac{m_D}{V_S}; \tag{10}$$

$$\rho_R = \frac{m_D}{V_R}; \tag{11}$$

$$\rho_B = \frac{m_D}{V_B} \tag{12}$$

The weight imbibition coefficient (IC_W) and the saturation index (SI) were computed as:

$$\text{IC}_W = \left[\frac{(m_W - m_D)}{m_D} \right] \cdot 100 \tag{13}$$

$$\text{SI} = \left(\frac{\Phi_{O\text{H}_2\text{O}}}{\Phi_{O\text{He}}} \right) = \left\{ \frac{\left[\frac{(m_W - m_D)}{\rho_{WTx}} \right]}{V_O} \right\} \cdot 100 \tag{14}$$

The punching strength index (PLT index) was determined on the same pseudo-cubic rock specimens used for other physical properties (porosity, density, water absorption, etc.) with a Point Load Tester (mod. D550 Controls Instrument), according to ISRM (1972, 1985). The load was exerted via the application of a concentrated load with two opposing conical punches. The resistance to puncturing (I_s) was calculated as:

$$I_s = \frac{P}{De^2} \quad (15)$$

where P is the breaking load and De is the “equivalent diameter of the carrot” (ISRM 1985), with:

$$De = \frac{4A}{\pi} \quad (16)$$

$$A = W \cdot D \quad (17)$$

where W and $2L$ are the width perpendicular to the direction of the load and the length of the specimen, respectively.

The index value is referred to a standard cylindrical specimen with diameter $D = 50$ mm for which I_s has been corrected with a shape coefficient (F) and calculated as:

$$I_{s50} = I_s \cdot F = I_s \cdot \left(\frac{De}{50}\right)^{0.45} \quad (18)$$

A testing machine (digital model 50-C54, Controls) was used to determine the uniaxial compressive strength (R_c) (according to UNI EN 1926 2007) and flexural strength (R_f) and on prismatic specimens with size $10 \times 50 \times 20$ mm (according to UNI EN 12372 2001). The specimens were dried at 60 ± 5 °C until stationary dry weight ($\Delta m_D < 1\%$). The strength measurements were acquired by using a Wizard Basic microprocessor digital readout unit. The compressive strength (R_c), determined with the load applied to the X – Y – Z sample axes, was calculated as:

$$R_c = \frac{P}{A} \quad (19)$$

where P is the breaking load and A is the area of the specimen section perpendicular to the direction of the load.

Ultrasonic testing has been effectuated on 12 cubic specimens side $50 \times 50 \times 50$ mm. The instrument used for the test is the Ultrasound Controls 58-E4800 according to the standards: UNI EN 12504-4 (2005) and ASTM C597 09 (2009). The ultrasonic velocity was calculated dividing the distance between the two parallel faces of the cubic shapes for the travelling time of the ultrasonic pulse through the two faces of the sample. The values of velocity was determined before treatment and after 24 h, 7 and 24 days, to monitor the degree of consolidation over the time, according to three main directions: (1) perpendicular

to the bedding planes/deposition of *Pietra Cantone* stone (axis Z); (2) parallel to the planes in the axis signed with X ; (3) parallel to the planes (and orthogonally to X) in the axis signed with Y .

The vapour permeability was determined according to NORMAL 21/85 (1985).

To measure the amount of water vapour diffused through the sample, the test is repeated at regular intervals of 24 h until reaching the steady state. That is considered achieved when the average value of the weight variation ΔM in the time interval of 24 h, considering three values recorded at 24, 48, 72 h in steady during which the ΔM showed an oscillation around to an average value $< 5\%$.

The water vapour permeability, so calculated, was then expressed in $g/m^2 \cdot 24$ h (according to ANSI-ASTM C355-64) and normalized to 20 °C.


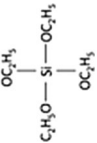
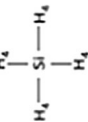
Treatment methods and chemicals characteristics

Two different consolidant and water repellent products are used, of which the data are reported in Table 1. All the specimens, before treatment, have been cleaned superficially by removing the fats resulting from sawing, and they were placed in the stove at 60 °C for 72 h. The consolidants were applied by immersion of the specimens in fibreglass becker for a duration of 24 h at an ambient temperature between 20 and 25 °C and relative humidity of 40–50% sheltered from sunlight to homogenize and ensuring complete absorption of the chemicals in the specimens and to obtain direct information on the maximum quantity absorbed by the sample. The nano-molecular hydrophobic was smeared with a paint brush.

Mineral Consolidant (commercial label, called from here CM) is a concentrated impregnating product of silicates, mainly potassium and sodium silicates in greater quantities in hydroalcoholic dilution (variable, in average 50%) at $pH = 11 \pm 0.5$. This solution forms a chemical reaction with the salts of the stone, and they stabilized binders forming Ca/Na/K-carbonates and amorphous silica. The silica has strong consolidating and aggregating capabilities, and the Si–O bond underlying the silica derivatives is very stable and therefore resistant to ageing. The low specific weight (1.056 g/cm³) in the formulation makes CM consolidant particularly pervasive in the walls: it is used as well as smoothing of grip to daub walls with lime (AA.VV. 2002; Spadola 2005). CM chemical needs an amount 350 g/m² according to the tests of Produzioni Freius Chimici srl company.

The hydrolysis of alkaline elements such as sodium leads to the formation of hydroxides, which are conveyed during the evaporation of the solvent that cause sub-efflorescence in the stone surface (Fig. 12a–d). Salts coming from consolidation with alkali-silicates are known in many

Table 1 Chemical and physical properties of consolidant and protective products

Chemicals	Stg	Use	Product class	Composition	Chemical formula	Typical bond	Conc. (%)	Dilution type	Specific weight (g/cc)	Aspect	pH
Mineral silicate	CM	Consolidant	Silicate	Solution of K, Li, Ba, Na silicates	K_2/Na_2SiO_3		Variable (30–60)	Hydroalcoholic	1.056	Colourless, odourless	11 ± 0.5
Ethyl silicate	FB	Consolidant	Alkoxysilanes	Ethyl ester solution of silicic acid	$Si(OC_2H_5)_4$		70	Alcoholic	0.970	Straw yellow, orange flavour	/
Nano-molecular gel	NG	Protective	Silane monomer	Silane monomer	SiH_4		43	Hydroalcoholic	± 1.000	White, odourless	7.5 ± 0.5 (amorphous state)/10 (solid state)

cases conservation to be the main reason for great damage on Cultural Heritage (see, e.g., Arnold and Zehnder 1991).

Ethyl Silicate Indurent (Indur FB, called from here FB) is a monocomponent product in alcoholic fluid dilution. It contains a percentage of ethyl silicate in a concentration of 70% with a specific weight of 0.97 g/cm³. On the basis of experience, it is suitable for the type of carbonate/calcareous stones. The product precipitates by hydrolysis following a reaction with atmospheric moisture that acts as a catalyst, forming ethyl alcohol as a secondary product. FB is an inorganic substance in low-molecular organic solvent, so it has a low viscosity and is highly penetrating. In fact, compared to water, ethanol is characterized by a lower surface tension and contact angle, and so a higher wetting ability. Ethyl Silicate is also used for surface protection of concrete (Franzoni et al. 2013).

The product penetrates as liquid phase, after about a week silica goes to viscose phase according to the sol-gel process (Sponchia 2011). Consolidation (Fig. 6k–n) is effectively complete after about 3–4 weeks from the treatment, when the silica gel will complete its transition to the amorphous solid state (Rodriguez Navarro et al. 1996). The synthesis of hybrid materials (silica + ethanol) based on sol-gel process allows to obtain the products in which the organic molecules are introduced and linked to inorganic bonds of the silica. In this way, it gives elasticity to the obtained gel that is less susceptible to crimp during the drying phase (Salazar Hernández et al. 2010).

The success of alkoxysilane consolidants on carbonate rocks is a topic of some debate. This formulation is widely used in the consolidation of siliceous rocks. In fact, some works dating back to the 1970 demonstrate that the properties of mechanical strength greater increase in the sandstones compared to carbonate rocks (Goins et al. 1996) because the structural and chemical characteristics of the stone condition the bonding ability of the ethyl ester. If the stone does not present –OH groups, the silica precipitates in the pores and fills the intergranular spaces by increasing the compressive strength, but it does not form a real pattern between the minerals disintegrated by reacting with the hydroxyl groups. Precisely, for this reason, it has been effective in the sandstones and clays, while you think it is not suitable for marble and limestone (Plenderleith and Werner 1973; Amoroso 2002). In limestones, the hydroxyl groups are bonded to the fraction of impurities (i.e., minerals such as illite and montmorillonite) which are present in the carbonate matrix. These impurities play an important role because they contain hydroxyl groups (about 10%) that are sufficient to bind colloidal silica to carbonate matrix (Mameli 2012), especially. Effectiveness of alkoxysilanes to bind to the mineral phases of the limestone will be studied. The Indur FB can be applied using an amount of 650 g/m² according to Produzioni Freius Chimici srl experience.

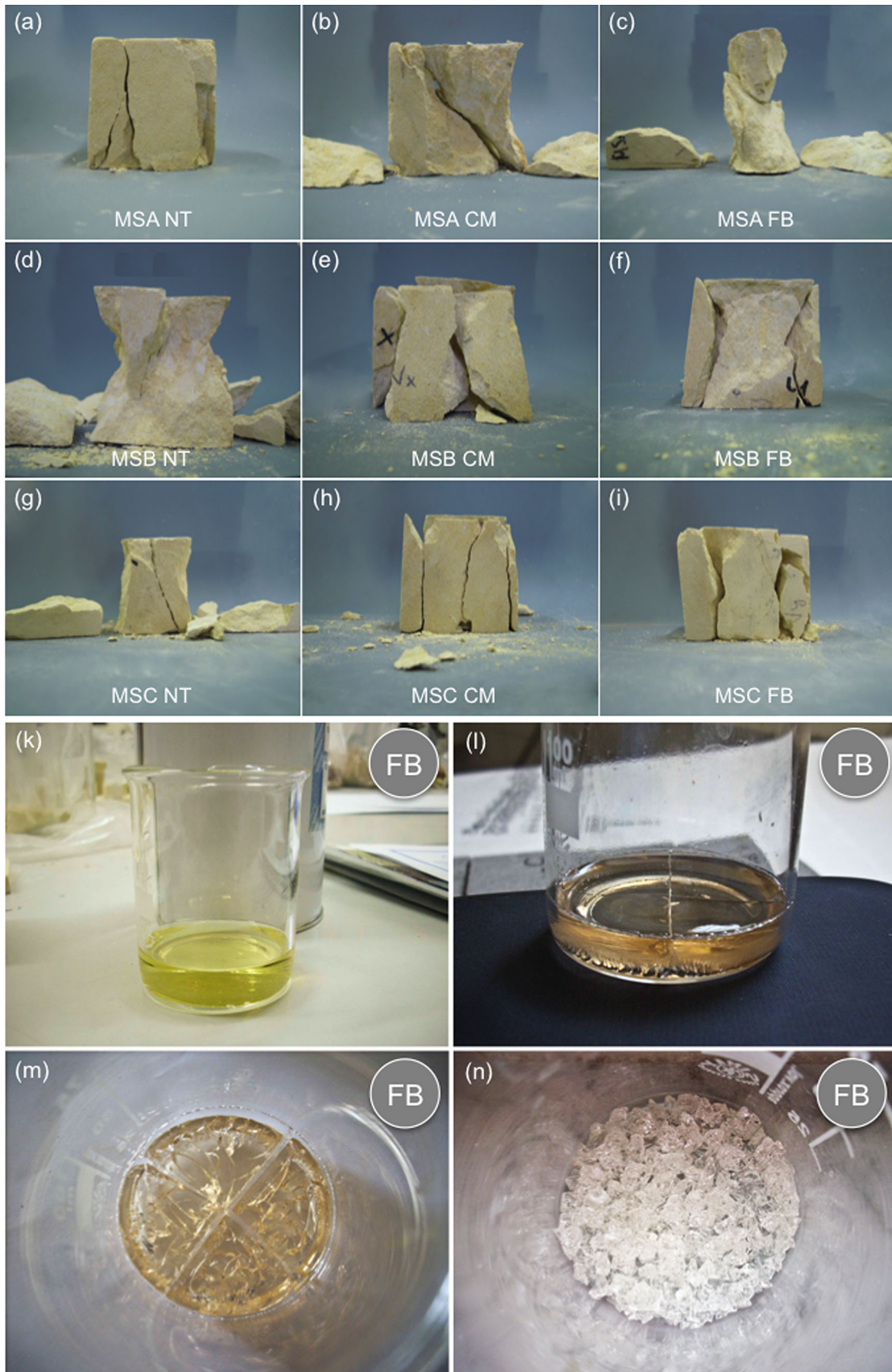


Fig. 6 Determination of compressive strength on cubic specimens with size $50 \times 50 \times 50$ mm with some specimens with typical hourglass rupture once exceeded the breaking load. **a** MSA-untreated sample; **b** MSA CM-treated sample; **c** MSA FB-treated sample; **d** MSB-untreated sample; **e** MSB CM-treated sample; **f** MSB FB-treated sample; **g** MSC-untreated sample; **h** MSC CM-treated; **i** MSC FB-treated. **k, l, m, n** INDUR FB consolidation: **k** chemical as liquid phase; **l** gel phase after 8 days; **m** hardening process about 14 days; **n** solid state of FB about 1 month (with amorphous SiO_2)

Protective treatments can yield the stone totally impermeable to water (waterproofing), or impermeable only to liquid water (water repelling) while allowing passage of water vapour (Gray 2000). The water repellent that has been used in this research is a nano-molecular gel based on Silane Monomer nano-molecular (alkyl alkoxy silane monomer, called from here NG) in hydroalcoholic dilution at $\text{pH} = 7/8$. Compared to other products (i.e., epoxy resins), it is distinguished by the small size of the molecules of the monomer equivalent to 10 \AA and low specific weight (about 1 g/cm^3), so it can dissolve in polar solvents such as alcohols or water (so it can also be applied to damp surfaces) creating a film not harmful and chemically anchored to support, able to make the material highly hydrophobic. Due to its chemical characteristic, the nano-molecular silane possesses a very high penetration, and it is therefore able to hydrophobise the smaller capillaries and to combat the penetration of chlorides and soluble salts. The polymerization of the monomer silane is initiated by a hydrolysis reaction. Hydrolysis is the chemical reaction of an alkoxy silane with water or with the hydroxyl groups ($-\text{OH}$) on the surface of a mineral grain. The hydrolysis reaction produces a silanol and an alcohol as a by-product, which rapidly evaporates. In the course of polymerization, this partially hydrolyzed molecule can then undergo either further hydrolysis or condensation (Ozturk 1992). Considered the probable loss of effectiveness over time (Wheeler 2005; Alfano et al. 2006; Lopez-Arce et al. 2009), and also in accord with its low molecular weight, the silane monomer was used in a concentration of 42–43% by weight. The silane condensation product comprises a three dimensional molecular network which is derived from reactive precursors or as applied precursors which provides protection to a porous substrate (Larry et al. 1996).

Results and discussion

Petrographic and compositional characteristics of *Pietra Cantone*

The three samples of *Pietra Cantone* limestone (i.e., MSA, MSB, MSC) show similar macroscopic characteristics with

a low or absent cementing degree. The MSA sample, unlike the other two samples, shows overall a greater presence of clay minerals compared to two other samples, represented by occasionally plaques placed sub-parallel to the sediment deposition (Fig. 3f).

The OM, XRD and SEM analysis highlight a similar composition of the MSA, MSB and MSC samples, characterized by a lime-mud supported matrix (Figs. 7a–d, 8), consisting of crystal-granules (with size mainly between 5 and $25 \mu\text{m}$; Fig. 8) of calcite (about 85–90 vol% of total granules; occasionally as well-developed crystals; Fig. 8), quartz (<3%), mica (mainly biotite and subordinate illite, <3%; Fig. 7e), K-feldspar (<2%), opaque (<2% with diameter $100\text{--}300 \mu\text{m}$; Fig. 7), rare montmorillonite and kaolinite. Crystal-clasts (15–20 vol% of rock, with variable origin and size, mainly from about $80\text{--}650 \mu\text{m}$) and bioclasts (20–25 vol% of rock, $>50 \mu\text{m}$; Figs. 7, 8d) are present. The bioclastic component consists of planktonic and benthonic foraminifera skeletons (30%, e.g., mostly Globigerinidae) and fragments of various shells (as elongated crinoid fragments), brachiopods (as curved fragments) (Fig. 7c, d), bryozoans and other. The presence of foraminifera typical of oxygenated clean sea-water at normal salinity indicates a sub-littoral deposition environment. The rock is affected by a fractures filled with spathic calcite.

According to Folk (1959) and Dunham (1962) classifications, the three samples of *Pietra Cantone* can be defined as biomicritic limestone and as wackestone, respectively. However, on the basis of microscopic observations and given the environment of deposition conditions, it is preferable to define them as marly limestones poorly cemented, with mainly muddy microcrystalline matrix and variable presence of bioclastic components.

XRD analysis show the occasionally presence of gypsum (as result of secondary sulfatation process of carbonate cement and/or also as sindepositional phase).

SEM analysis on external surface of untreated samples (Fig. 8) shows a crystalline micrometric structure mainly consisting of granules of calcite ($>85 \text{ vol}\%$) with size range $1\text{--}10 \mu\text{m}$ and frequently between 1 and $3 \mu\text{m}$. The subordinate presence of quartz ($8\text{--}10 \mu\text{m}$; Fig. 7e), K-feldspar ($10\text{--}20 \mu\text{m}$; Fig. 8a, b), biotite ($4\text{--}12 \mu\text{m}$), illite ($10\text{--}15 \mu\text{m}$; Fig. 7e) is observed. Rare apatite crystals ($25 \mu\text{m}$), bioclastic fragments ($20\text{--}30 \mu\text{m}$; Fig. 8d) and mixed chlorides of Ca/K/Na ($8\text{--}15 \mu\text{m}$) are present. These latter are original salts of marine deposition.

The SEM microphotographs of Fig. 8c–f show the intergranular contacts and crystal habit of the grains, in some cases idiomorphic (e.g., calcite), and low cementation degree of matrix where the grains are joined together through to the interlocking of the phases rather than the cohesion forces.

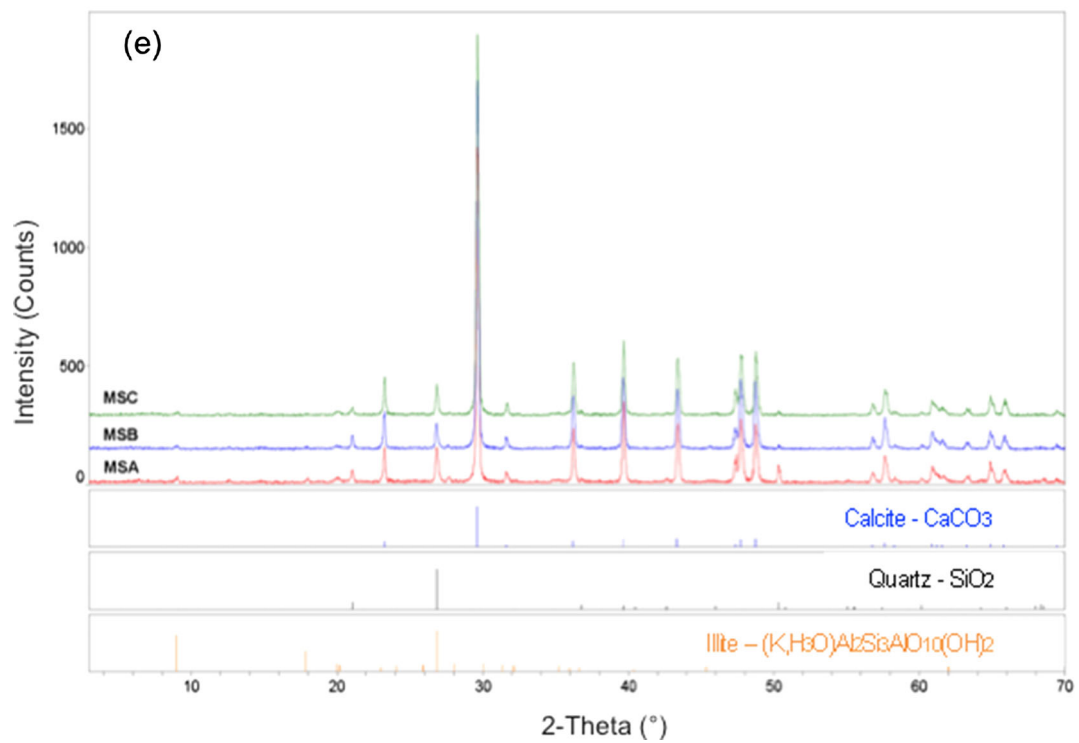
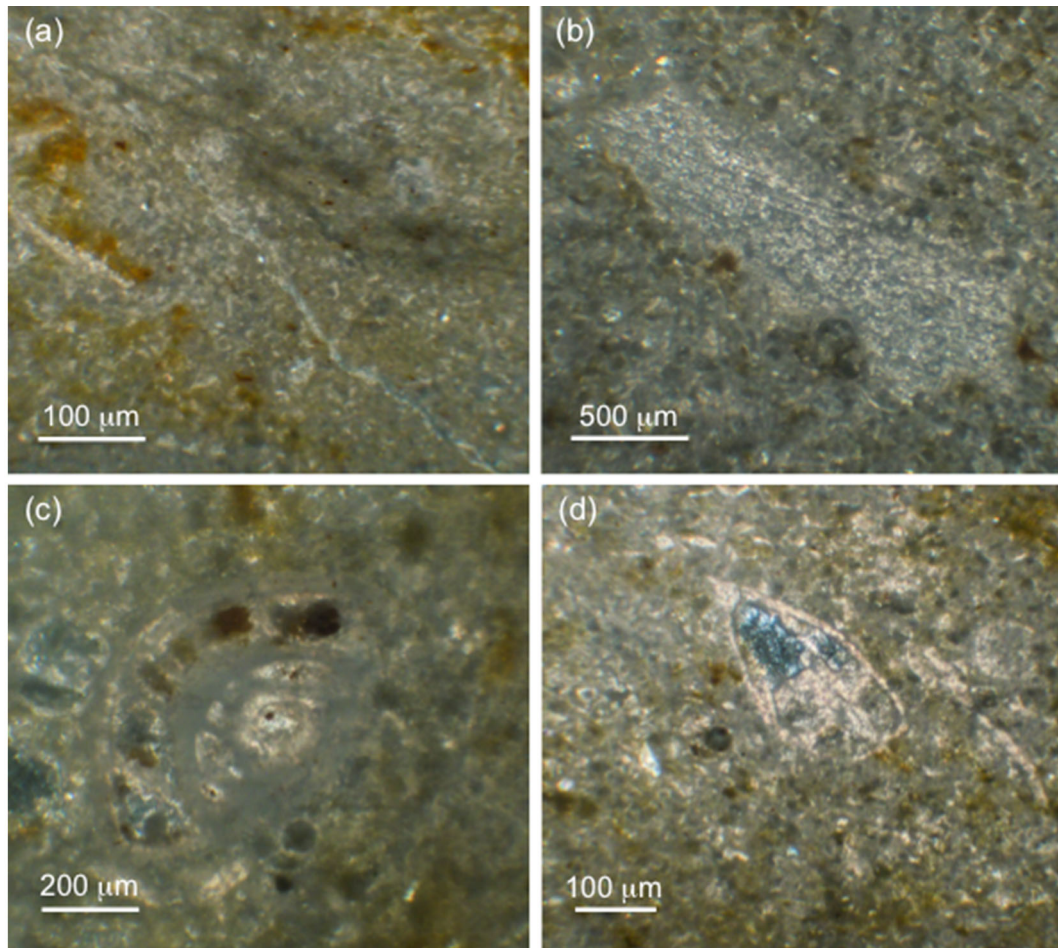


Fig. 7 **a, b, c, d** *Pietra Cantone* thin sections, crossed Nicols: **a** red-brown interbedding claysh layer; **b** patch; **c, d** detail of *Globigerinidae* and fragments of various shells (crinoids, brachiopods); **e** X-ray diffraction analysis (XRD): presence of calcite, quartz and phyllosilicates (i.e., illite group) and relative standard peaks

Physical–mechanical properties and decay of *Pietra Cantone*

The helium picnometry analysis on all analysed specimens highlights a maximum range of total porosity between 28 and 36 vol% (Tables 2, 3; Fig. 9), with following means: $32.52 \pm 1.46\%$ in MSA sample, $32.59 \pm 0.51\%$ in MSB sample and $33.76 \pm 1.18\%$ in MSC sample (Table 3). The closed porosity shows low values (<0.7%). The bulk

density, inversely related to the total porosity and affected by the composition and fabric of stone, ranges between 1.76 and 1.96 g/cm^3 (Tables 2, 3; Fig. 9b).

SEM analysis shows an almost uncemented rock microstructure, where the grains are held together practically by van der Waals forces and interlocking. The observations at the micrometric scale highlight the presence of intergrain macropores frequently varying in the range of $5\text{--}50 \text{ }\mu\text{m}$ (Fig. 6e), and occasionally also $>50 \text{ }\mu\text{m}$ (Fig. 8f).

These data accord to the Hg-porosimetry analysis of Atzeni et al. (2006) made on the unaltered samples of *Pietra Cantone*, which highlight a similar mean of porosity: $34.19 \pm 3.45\%$. These latter data are lightly higher with

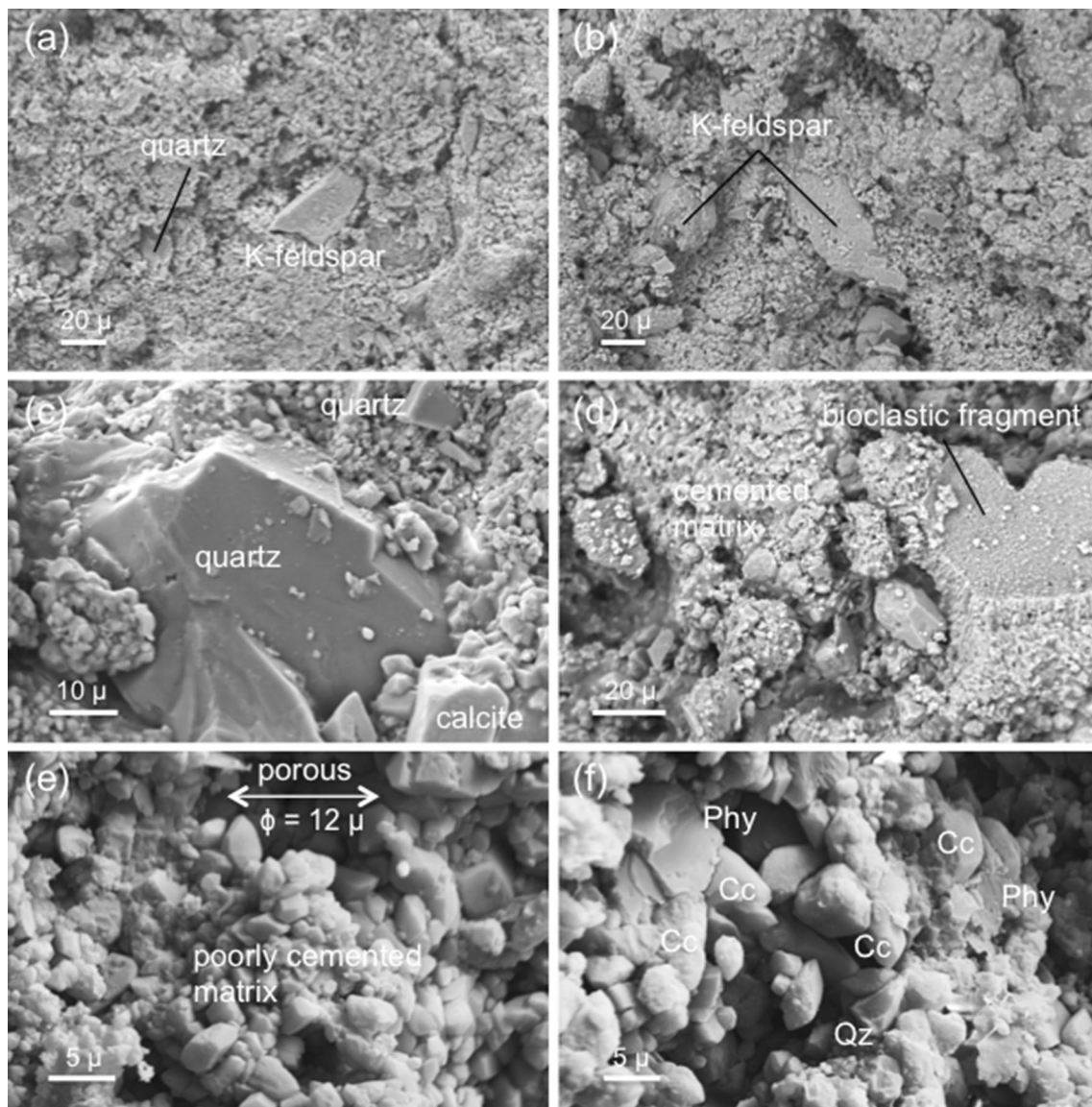


Fig. 8 SEM microphotographs of untreated samples: **a, b** quartz and K-feldspar crystals immersed in (mainly calcite) muddy matrix; **c** detail of quartz and calcite crystals; **d** bioclastic fragment immersed

in muddy medium cemented matrix; **e** view of porous poorly cemented matrix; **f** phyllosilicate, calcite and quartz crystals with diameter $< 10 \text{ }\mu\text{m}$

Table 2 Physical data of untreated samples (with size $5 \times 5 \times 5$ cm) of *Pietra Cantone* limestone

Sample	ρ_B g/cm ³	$\Phi_{O_2H_2O}$ %	Φ_C %	Φ_T %	$V_P X$ m/s	$V_P Y$ m/s	$V_P Z$ m/s	Anisotropy ratio			Anisotropy mean	V_P mean m/s
								X-Z	X-Y	Y-Z		
MSA 1	1.83	33.24	0.44	33.68	1992	1563	1223	1.63	1.27	1.28	1.39	1592
MSA 2	1.80	33.81	0.39	34.20	803	678	553	1.45	1.18	1.23	1.29	678
MSA 3	1.94	28.22	0.67	28.89	936	911	613	1.53	1.03	1.49	1.35	820
MSA 4	1.96	27.89	0.55	28.43	1672	813	795	2.10	2.06	1.02	1.73	1093
MSA 5	1.85	31.75	0.56	32.30	1931	1841	1260	1.53	1.05	1.46	1.35	1677
Mean	1.88	30.98	0.52	31.50	1467	1161	889	1.65	1.32	1.29	1.42	1172
SD	0.07	2.78	0.11	2.69	560	510	334	0.26	0.43	0.19	0.18	449
MSB 1	1.88	31.82	0.25	32.07	1939	802	668	2.90	2.42	1.20	2.17	1137
MSB 2	1.81	33.62	0.56	34.18	832	747	652	1.28	1.11	1.15	1.18	744
MSB 3	1.87	30.91	0.59	31.50	1449	1304	923	1.57	1.11	1.41	1.37	1225
MSB 4	1.88	30.82	0.63	31.45	1316	1021	742	1.77	1.29	1.38	1.48	1026
MSB 5	1.78	34.89	0.43	35.31	1119	914	901	1.24	1.22	1.01	1.16	978
Mean	1.84	32.41	0.49	32.90	1331	958	777	1.75	1.43	1.23	1.47	1022
SD	0.05	1.78	0.16	1.75	412	220	128	0.68	0.56	0.17	0.41	183
MSC 1	1.88	31.36	0.26	31.62	1534	996	599	2.56	1.54	1.66	1.92	1043
MSC 2	1.97	27.05	0.92	27.98	770	848	919	1.19	1.08	1.10	1.13	846
MSC 3	1.90	29.75	0.52	30.27	1871	1081	901	2.08	1.73	1.20	1.67	1285
MSC 4	1.93	29.09	0.64	29.74	1327	906	784	1.69	1.46	1.16	1.44	1006
MSC 5	1.83	31.93	0.77	32.70	1692	1222	837	2.02	1.38	1.46	1.62	1250
Mean	1.90	29.84	0.62	30.46	1439	1011	808	1.91	1.44	1.32	1.56	1086
SD	0.05	1.94	0.25	1.81	424	148	129	0.51	0.24	0.24	0.30	182

Legend symbols: ρ_B , bulk density; $\Phi_{O_2H_2O}$, helium open porosity; Φ_C , water closed porosity; Φ_T , total porosity; $V_P X$, longitudinal wave ultrasonic velocity measured on X axis; $V_P Y$, longitudinal wave ultrasonic velocity measured on Y axis; $V_P Z$, longitudinal wave ultrasonic velocity measured on Z axis; V_P mean, longitudinal wave ultrasonic velocity average between X, Y, Z axes

respect to those determined in this work with helium picnometry, probably because the high pressure of Hg-intrusion method has generated a partial fragmentation of micrometric porous network in these rocks. The increase in porosity values due to a microstructural crushing at high Hg-pressure is known in the literature. Some authors (Zinsmeister et al. 2012) have showed this discrepancy by using a comparison with Nuclear Magnetic Resonance (NMR) method. Hg-porosimetry analysis of Atzeni et al. (2006) on unaltered samples show a broad pore size asymmetric unimodal distribution ranging over five size orders, where 70% of the total porosity fall into the 1–16 μm size range, 10% in the 16–32 μm range and about 20% of total porosity lower to 1 μm . The modal size range is 8–16 μm , with about 30% of total porosity. The inter-grain macropores with size >32 μm observed in SEM analysis on the surfaces of the MSA, MSB, MSC samples probably are due to greater physical alteration of monument samples analysed, which lead to the detachment of the crystalline granules.

Moreover, to characterize the distribution of porosity with size <0.18 μm (1800 \AA), N₂ porosimetry analysis was made on outgassed samples of *Pietra Cantone*. No

differences were observed in the porous network of the three lithotypes MSA, MSB and MSC samples. Figure 10a, b shows the isotherm and the pore distribution of MSB sample. The limestone shows an isotherm (Fig. 10a), classified as type IV hysteresis loops according to the IUPAC classifications (Sing et al. 1985), due to mesoporous adsorbents. No contribution from the micropores connecting the mesopores was found for any of the studied materials. The calculated pore volume and the specific surface area values are 0.019469 cm³/g and 10.9920 m²/g, respectively. The porosity is mainly distributed on the range 15–1800 \AA (i.e., 0.0015–0.18 μm), with a main peak around 37 \AA (Fig. 10b). According to IUPAC pore classification (Sing et al. 1985), the porosity mainly fall in macro- and mesopore size ranges.

The physical characteristics of *Pietra Cantone* change as function of the depositional compaction and alteration, which affects especially the porosity and mechanical strength. The alteration degree of monument limestone depends on: (1) original depth in the stratigraphic sequence of *Pietra Cantone* formation (Barroccu et al. 1981), (2) compositional characteristics, i.e., variable presence of the clay terrigenous components, (3) microenvironmental

Table 3 Physical properties of the limestone: ρ_S , solid volume; ρ_R , real density; ρ_B , bulk density; Φ_{OHe} , He open porosity; Φ_{CHe} , He closed porosity; Φ_{OH_2O} , H₂O open porosity; Φ_T , total porosity; IC_W , water-imbibition coefficient; SI, saturation index

Sample	Physical state	ρ_R (g/cm ³)	ρ_S (g/cm ³)	ρ_B (g/cm ³)	Φ_{OHe} (%)	Φ_{CHe} (%)	Φ_{OH_2O} (%)	Φ_T (%)	IC_W (%)	SI (%)
MSA 1	Untreated	2.7381	2.7565	1.8305	33.15	0.45	32.47	33.59	17.74	98.24
MSA 2		2.7250	2.7413	1.8597	31.75	0.41	31.36	32.16	16.86	99.05
MSA 3		2.7056	2.7309	1.7901	33.84	0.61	32.90	34.45	18.38	97.52
MSA 4		2.7171	2.7378	1.8823	30.72	0.52	30.19	31.25	16.04	98.54
MSA 5		2.7151	2.7374	1.8850	30.57	0.57	29.63	31.14	15.72	97.19
	Mean	2.7202	2.7408	1.8495	32.01	0.51	31.31	32.52	16.95	98.11
	SD	0.0122	0.0096	0.0398	1.45	0.09	1.41	1.46	1.12	0.75
MSA NG1	Nano-gel treated	2.7080	2.7302	1.8592	31.34	0.56	4.07	31.90	2.19	13.02
MSA NG2		2.7219	2.7451	1.8605	31.65	0.58	4.30	32.23	2.31	13.64
MSA NG3		2.7017	2.7204	1.8242	32.48	0.46	4.76	32.94	2.61	14.70
MSA NG4		2.7106	2.7337	1.8404	32.10	0.57	4.27	32.68	2.32	13.33
MSA NG5		2.7534	2.7701	1.7975	34.72	0.39	4.27	35.11	2.38	12.35
	Mean	2.7191	2.7399	1.8364	32.46	0.51	4.33	32.97	2.36	13.41
	SD	0.0205	0.0191	0.0264	1.34	0.08	0.26	1.26	0.16	0.87
MSB 1	Untreated	2.7512	2.7613	1.8681	32.10	0.25	30.75	32.35	16.46	96.07
MSB 2		2.7235	2.7468	1.8491	32.10	0.58	31.23	32.68	16.89	97.55
MSB 3		2.7079	2.7310	1.8608	31.28	0.58	31.29	31.86	16.81	99.38
MSB 4		2.7236	2.7487	1.8463	32.21	0.62	31.71	32.83	17.18	98.74
MSB 5		2.7327	2.7508	1.8371	32.77	0.44	32.55	33.22	17.72	99.62
	Mean	2.7278	2.7477	1.8523	32.09	0.49	31.51	32.59	17.01	98.27
	SD	0.0159	0.0109	0.0122	0.53	0.15	0.68	0.51	0.47	1.47
MSB NG1	Nano-gel treated	2.7501	2.7692	1.8381	33.16	0.46	5.05	33.62	2.75	15.28
MSB NG2		2.7164	2.7405	1.8798	30.80	0.61	5.07	31.41	2.70	16.50
MSB NG3		2.7180	2.7425	1.8766	30.96	0.62	4.84	31.57	2.58	15.68
MSB NG4		2.7300	2.7467	1.8508	32.20	0.41	4.70	32.62	2.54	14.64
MSB NG5		2.7050	2.7313	1.8835	30.37	0.67	4.26	31.04	2.26	14.06
	Mean	2.7239	2.7460	1.8658	31.50	0.55	4.78	32.05	2.56	15.23
	SD	0.0171	0.0141	0.0201	1.15	0.11	0.33	1.06	0.19	0.94
MSC 1	Untreated	2.7403	2.7507	1.8112	33.91	0.25	33.60	34.16	18.55	99.39
MSC 2		2.7009	2.7355	1.7620	34.76	0.83	33.49	35.59	19.01	96.62
MSC 3		2.7079	2.7280	1.8364	32.18	0.50	31.92	32.68	17.38	99.48
MSC 4		2.7200	2.7449	1.8239	32.94	0.61	32.09	33.55	17.59	97.69
MSC 5		2.6953	2.7263	1.8311	32.06	0.77	31.71	32.83	17.32	99.19
	Mean	2.7129	2.7371	1.8129	33.17	0.59	32.56	33.76	17.97	98.48
	SD	0.0179	0.0106	0.0300	1.15	0.23	0.91	1.18	0.76	1.27
MSC NG1	Nano-gel treated	2.7065	2.7302	1.8831	30.42	0.61	4.25	31.03	2.26	14.01
MSC NG2		2.7137	2.7432	1.8508	31.80	0.73	3.71	32.53	2.00	11.70
MSC NG3		2.7203	2.7405	1.8905	30.50	0.51	3.30	31.01	1.74	10.85
MSC NG4		2.7120	2.7252	1.8178	32.97	0.33	3.09	33.30	1.70	9.39
MSC NG5		2.7273	2.7521	1.8773	31.17	0.62	3.67	31.79	1.96	11.82
	Mean	2.7159	2.7382	1.8639	31.37	0.56	3.60	31.93	1.93	11.55
	SD	0.0080	0.0107	0.0298	1.05	0.15	0.45	0.99	0.22	1.68

SD standard deviation

conditions and decay processes that occur after the laying of stone in the monument. In fact, due to the presence of clay minerals (i.e., phyllosilicates) and salts (e.g., gypsum, Na-carbonates, NaCl, etc.), this limestone is easily

degradable at the presence of air humidity or water circulation. Moreover, considering the high value of permeability ($K = 1.481 \times 10^{-13}/m^2$, equivalent to 1480 millidarcy, with K according to Darcy's law; Atzeni et al.

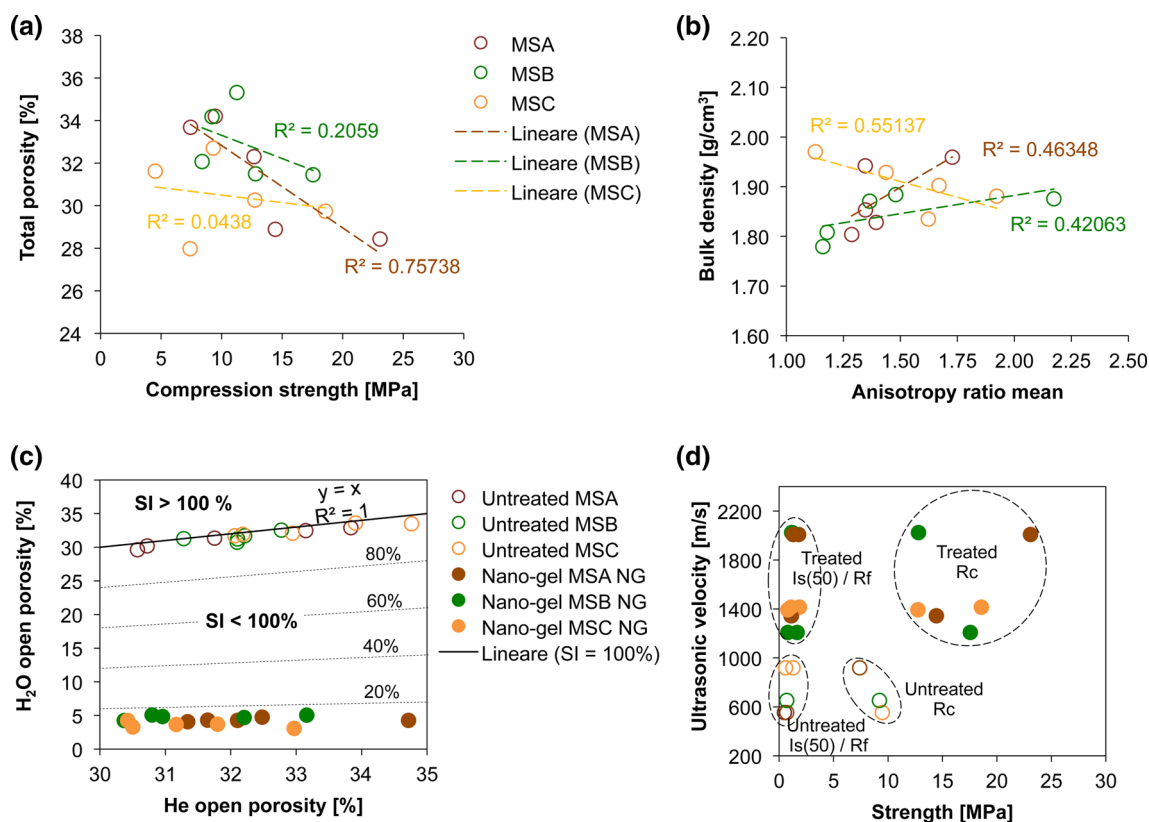


Fig. 9 Physical properties of *Pietra Cantone* limestone. **a** compressive strength versus total porosity of untreated cubic samples with size $5 \times 5 \times 5$ cm; **b** anisotropy ratio mean versus bulk density; **c** He open porosity versus H_2O open porosity of untreated and nano-gel-

treated samples where has been showed the saturation index fields ($SI >$ or $< 100\%$); **d** punching, compressive, flexion strength versus ultrasonic velocity of untreated and treated samples with CM and FB consolidants

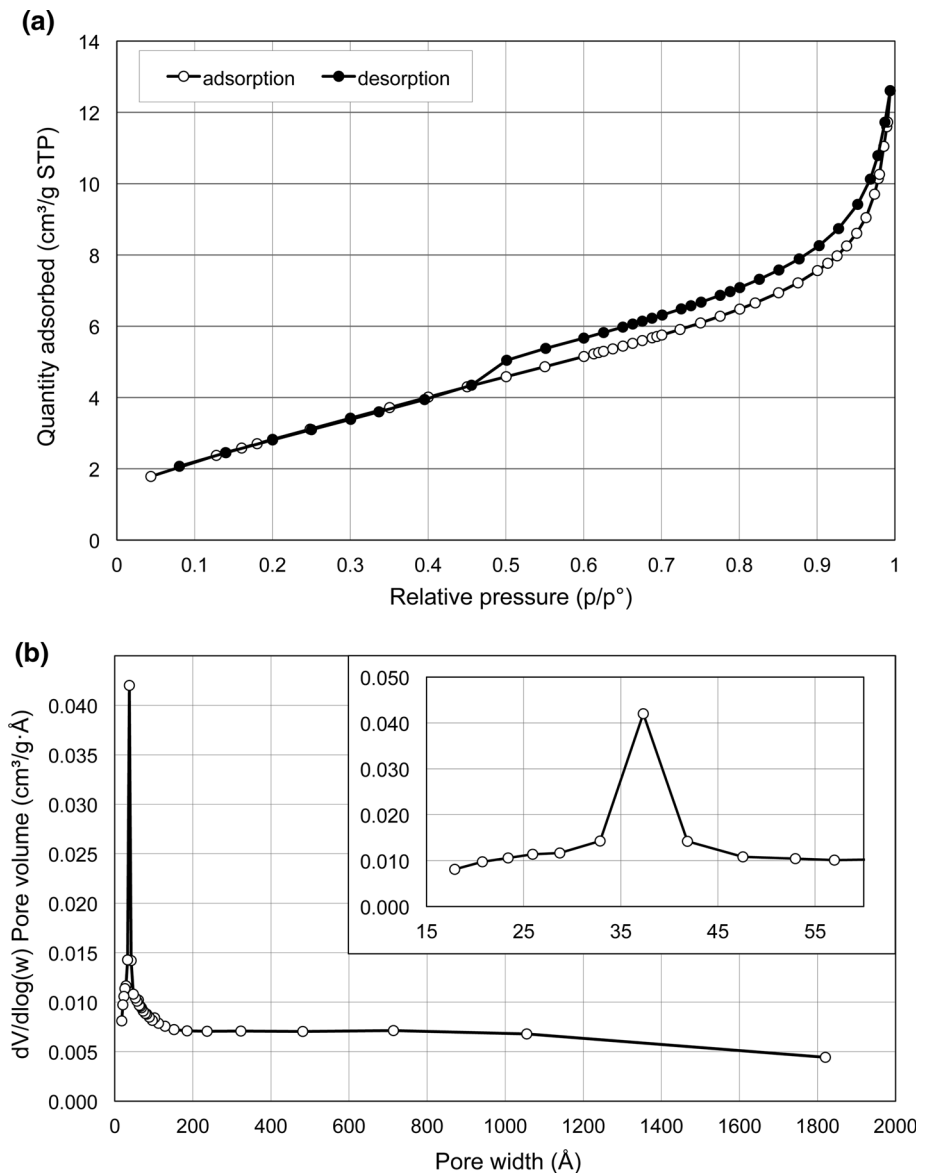
2006), the circulating aqueous solutions, especially in the stone ashlar of basal walls (with height < 1 m) where the capillary rise is frequently present, constitute an even more dangerous factor for the physical decay of the limestone (Fig. 3). Within the stone, the continuous cyclic processes of solubilization/crystallization of soluble salts and/or hydration/dehydration of hygroscopic phases (e.g., salts, phyllosilicates that when wet expands to many times its volume; Brown 1961) produce a reversible hydric dilatation of stone ashlar and consequent destructive effects inside the porous matrix (Guerrero et al. 1990; Zezza et al. 1990). In other cases, for example when the stone surface is directly exposed to weathering and especially to acid rain, the decay of porous limestone, as the case of *Pietra Cantone*, is also due to the dissolution of the carbonate cement and calcite microcrystals of matrix.

All these processes often lead to an increase in porosity and a decrease in bulk density and mechanical strength (e.g., compressive resistance; Atzeni et al. 2006). Moreover, the presence, internally the stone, of elongated clay patches (Fig. 3f) creates microstructural plans of physical–mechanical weakness, decreasing significantly the strength. This is highlighted by some low value of

compressive strength in MSA with respect to the mean (Table 2), low PLT index (Table 6) and by higher standard deviation of ultrasonic velocity (with V_p means of 446 m/s in MSA versus 183 and 182 m/s in MSB and MSC; Table 2).

The samples which have been taken from the monument and examined in this paper show a certain variability of physical data, especially high total porosity, also inside the same lithotype, due to a compositional heterogeneity and a variable alteration degree. The decay of monument samples is highlighted also by low and variable values of ultrasonic velocity of longitudinal waves ($V_p = 553 \div 1260$ m/s, range on Z axis, orthogonal to stratigraphy; Table 2) compared to those of unaltered limestone taken from quarry ($V_p \approx 2100 \div 3600$ m/s; Cuccuru et al. 2014; Concu et al. 2014). This evidently shows the presence of physical decohesion of matrix (Fig. 6) and probably also physical discontinuities due to the pressure of static load of masonry (e.g., microfissures) and to compositional inhomogeneity (Fig. 3f). The different velocity values, which have been measured on three main axis (X, Y, Z; Table 2), show two constant anisotropy degrees (mainly X–Z and minor X–Y; Fig. 9b) of *Pietra Cantone* limestone.

Fig. 10 Porosimetry by BET and BJH methods on untreated *Pietra Cantone* (samples MSB). **a** nitrogen sorption isotherm at 77 K of adsorption and desorption; **b** distribution of pores with diameter < 0.18 μm; the mesopore size distribution was derived from the Barrett–Joyner–Halenda (BJH) method (Barrett et al. 1951)



The compressive strength values are equally low (4.5–9.5 MPa, with load on Z axis; Table 2; Fig. 9a), with values under the frequent ranges of unaltered samples taken from quarry (10 ÷ 14 MPa, Cocco et al. 2015) and slightly altered samples (5 ÷ 11 MPa, Concu et al. 2014). However, the values do not reach those of strongly altered samples taken at the surface of the outcrops (0.4 ÷ 0.8 MPa, Barroccu et al. 1981).

Protective efficacy

To verify the efficacy of the nanotechnology product, the data of open porosity to gas-helium (Φ_{OHe}), open porosity to liquid-water (Φ_{OH_2O}), vapour permeability at steady state are analysed before and after chemical treatment. Given the poor resistance of *Pietra Cantone* limestone, due

to both the intrinsic characteristics of the material and a slight degree of rock alteration, the water absorption tests by total immersion were interrupted at 72 h to avoid loss of material for decohesion. The results were, however, useful in assessing the effectiveness of protective chemical.

The helium open porosity of untreated samples has values lightly less respect to the total porosity (Table 3; Fig. 9c, d) varying between about 28 and 35%. The average values of MSA and MSB samples are similar ($\Phi_T = 32.5 \pm 1.5$ and $32.6 \pm 0.51\%$, respectively), while MSC samples (more altered) show slightly higher values ($\Phi_T = 33.8 \pm 1.2\%$). Closed porosity is always <1% (Table 3). Open porosity to water, weight imbibition coefficient and saturation index (Fig. 9c) of untreated samples has different values with respect to the treated samples.

Table 4 Vapour permeability test of MSA, MSB and MSC limestones on untreated samples and treated samples with NG water repellent and CM–FB consolidants

Sample	Measures	Time interval (h)	Progressive total weight (g)	$\Delta M_p \cdot t =$ Progressive loss H_2O		Progressive vapour flux ($g/m^2 \cdot t$)	
				(g)	(%)		
(a)							
MSA untreated	0	0	182.77	0.0000	0.0000		
	1	24	182.15	0.6247	0.3418	9.2992	
	2	48	181.53	1.2356	0.6760	18.3931	
	3	72	181.02	1.7543	0.9598	26.1144	
	4	96	180.46	2.3054	1.2614	34.3180	
	5	120	179.98	2.7863	1.5245	41.4767	
	6	140	179.33	3.4384	1.8813	51.1838	
MSA CM	0	0	181.58	0.0000	0.0000		
	1	24	181.06	0.5200	0.2864	7.7407	
	2	48	180.52	1.0600	0.5838	15.7791	
	3	72	180.08	1.5000	0.8261	22.3289	
	4	96	179.58	2.0000	1.1014	29.7719	
	5	120	179.18	2.4000	1.3217	35.7262	
	6	140	178.61	2.9700	1.6356	44.2112	
MSA FB	0	0	172.08	0.0000	0.0000		
	1	24	171.64	0.4393	0.2553	6.5394	
	2	48	171.16	0.9232	0.5365	13.7427	
	3	72	170.60	1.4781	0.8590	22.0029	
	4	96	170.06	2.0173	1.1723	30.0294	
	5	120	169.77	2.3068	1.3405	34.3389	
	6	140	169.15	2.9311	1.7033	43.6321	
MSA NG	0	00	180.38	0.0000	0.0000		
	1	24	179.74	0.6400	0.3548	9.5270	
	2	48	179.10	1.2800	0.7096	19.0540	
	3	72	178.50	1.8800	1.0422	27.9855	
	4	96	178.02	2.3600	1.3083	35.1308	
	5	120	177.48	2.9000	1.6077	43.1692	
	6	140	176.85	3.5300	1.9570	52.5473	
(b)	0	0	176.26	4.1200	2.2841	61.3300	
	MSB untreated	0	0	195.45	0.0000	0.0000	
		1	24	194.99	0.4553	0.2329	6.7776
		2	48	194.48	0.9677	0.4951	14.4051
		3	72	194.04	1.4099	0.7214	20.9877
		4	96	193.56	1.8872	0.9656	28.0927
		5	120	193.19	2.2566	1.1546	33.5916
6		140	192.66	2.7922	1.4286	41.5645	
7	164	192.09	3.3588	1.7185	49.9988		

Table 4 continued

Sample	Measures	Time interval (h)	Progressive total weight (g)	$\Delta M_p \cdot t =$ Progressive loss H ₂ O		Progressive vapour flux (g/m ² ·t)
				(g)	(%)	
MSB CM	0	0	173.00	0.0000	0.0000	
	1	24	172.50	0.5042	0.2914	7.5055
	2	48	171.96	1.0444	0.6037	15.5469
	3	7	171.50	1.4969	0.8653	22.2827
	4	96	171.00	1.9971	1.1544	29.7287
	5	120	170.60	2.4015	1.3882	35.7486
	6	140	170.04	2.9576	1.7096	44.0266
MSB FB	0	0	175.27	0.0000	0.0000	
	1	24	174.84	0.4319	0.2464	6.4292
	2	48	174.13	1.1378	0.6492	16.9372
	3	72	173.69	1.5813	0.9022	23.5391
	4	96	173.12	2.1462	1.2245	31.9482
	5	120	172.83	2.4413	1.3929	36.3410
	6	140	172.14	3.1255	1.7832	46.5260
MSB NG	0	0	179.63	0.0000	0.0000	
	1	24	179.10	0.5255	0.2925	7.8226
	2	48	178.54	1.0914	0.6076	16.2465
	3	72	178.06	1.5739	0.8762	23.4290
	4	96	177.53	2.1022	1.1703	31.2932
	5	120	177.12	2.5122	1.3985	37.3964
	6	140	176.52	3.1082	1.7303	46.2684
(c) MSC untreated	0	0	178.48	0.0000	0.0000	
	1	24	177.33	1.1459	0.6420	17.0578
	2	48	176.91	1.5674	0.8782	23.3322
	3	72	176.10	2.3796	1.3333	35.4225
	4	96	175.40	3.0846	1.7283	45.9171
	5	120	174.67	3.8121	2.1359	56.7466
	6	140	173.93	4.5482	2.5483	67.7042
MSC CM	0	0	183.79	0.0000	0.0000	
	1	24	183.42	0.3684	0.2004	5.4840
	2	48	182.98	0.8143	0.4431	12.1216
	3	72	182.53	1.2563	0.6836	18.7012
	4	96	182.16	1.6273	0.8854	24.2239
	5	120	181.75	2.0359	1.1077	30.3063
	6	140	181.34	2.4526	1.3345	36.5092
	7	164	180.96	2.8350	1.5425	42.2016

Table 4 continued

Sample	Measures	Time interval (h)	Progressive total weight (g)	$\Delta m_p \cdot t =$ Progressive loss H ₂ O		Progressive vapour flux (g/m ² ·t)
				(g)	(%)	
MSC FB	0	0	180.24	0.0000	0.0000	
	1	24	179.87	0.3708	0.2057	5.5197
	2	48	179.32	0.9243	0.5128	13.7591
	3	72	178.70	1.5373	0.8529	22.8841
	4	96	178.16	2.0788	1.1534	30.9449
	5	120	177.61	2.6251	1.4564	39.0770
	6	140	177.10	3.1432	1.7439	46.7894
MSC NG	0	0	186.63	0.0000	0.0000	
	1	24	186.27	0.3597	0.1927	5.3545
	2	48	185.74	0.8858	0.4746	13.1860
	3	72	185.21	1.4189	0.7603	21.1216
	4	96	184.78	1.8546	0.9937	27.6074
	5	120	184.30	2.3299	1.2484	34.6827
	6	140	183.82	2.8145	1.5081	41.8964
	7	164	183.36	3.2719	1.7531	48.7053

Tables show the measurement of progressive total weight of specimens at regular intervals of 24 h. Progressive loss of H₂O (expressed in gram and %) allows to calculate the progressive vapour flux traversing specimens with of 50 × 50 × 10 mm in function of time

SD standard deviation

After chemical treatment with nano-gel, the same samples show similar values of physical properties (i.e., total, He open porosity, closed porosity and density; Table 3), while the water open porosity (and consequently the imbibition coefficient) shows a significant decrease (Table 3) that varies from ~85% in samples MSA NG and MSB NG, to 89% in samples MSC NG. Also, the saturation index shows a significant decrease (Fig. 9c; Table 3).

These results indicate that the nanotechnology chemicals are strong water-repellents, without altering the intrinsic properties of material (e.g., real density, total porosity, etc.). In fact, this product creates only a superficial film that rejects the penetration of water in liquid phase. In effect, absorption of this latter decreases, leaving unaltered the permeability to gaseous phases of the porous network, as highlighted by the graphic of vapour permeability tests (Table 4a–c; Fig. 11). The permeability averages vary from ~0.45 g/m²·24 h in the MSB, to ~0.56 g/m²·24 h in MSA, to ~0.76 g/m²·24 h in MSC, as function of open porosity and decay degree of stones. Except MSC samples that show a light decrease in permeability after treatment, in MSA and MSB samples, the permeability has increased with an improvement traversing of H₂O in the porous network, as highlighted by a lower angular coefficient of the representative straight line of untreated samples with respect to those of samples which have been treated with nano-gel (Fig. 11).

SEM analysis (Fig. 12h) shows the presence of coating nano-gel that covers the outer surface of the material making it water repellent. In the weeks after the treatments with “wet stone effect”, when solvent evaporation is not completed, any change of colour is visible on the outer surface. However, between the crystalline matrixes substantially composed of calcite, crystal patches are present with greater presence of the nano-gel coating, therefore with a non-homogeneous distribution of the chemical due to a different surface absorption. Figure 12h also shows a phyllosilicate crystal of smectite group.

Consolidating efficacy

The efficacy of the two consolidation treatments by immersion in the *Pietra Cantone* limestone was assessed by a comparison before and after the treatment with chemicals of following physical properties: ultrasonic velocity, resistance to punching strength $I_{s(50)}$ (PLT index), compressive (Rc) and flexural strength (Rf).

The ultrasonic velocity shows substantially the degree of compactness and indirectly a decrease or increase in the porosity. Moreover, the measurement of this property at regular time intervals allows to verify the variations of strength in time post-consolidation, after several days.

The ultrasonic velocity results (V_p) before treatment and after treatment (at 24 h, 8 and 15 days; Tables 2, 5;

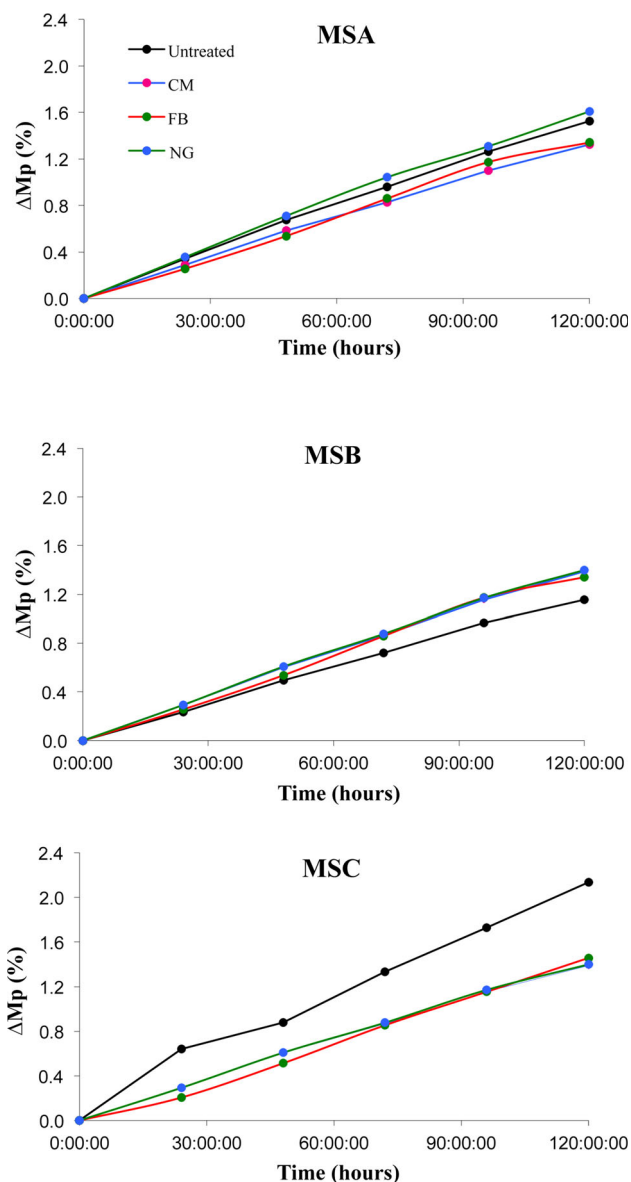


Fig. 11 Water vapour permeability test of untreated and treated MSA, MSB, MSC samples of limestone. ΔM_p (%) = percentage of progressive loss of vapour water is expressed in function of time. MSA: nano-gel protection causes an improvement of aqueous vapour flux in the porous network better than untreated and consolidated specimens. This latter shows a reduction of traversing of H_2O . MSB: The graph shows the similar progressive loss of water traversing treated samples. Vapour flux is higher in protected sample with water nano-gel repellent, while untreated sample has the lowest breathability. MSC: The water traversing in porous network of untreated sample shows that is much higher than those treated. The *straight line* of specimens coated with nano-gel repellent and consolidated with CM consolidant overlap, and their trend is similar to the consolidated sample with Indur FB

Figs. 9d, 13) highlight an improvement of the compactness of specimens (MSA, MSB and MSC) treated with CM and FB chemicals, although with some differences between two chemicals and direction of velocity measurement. Due to

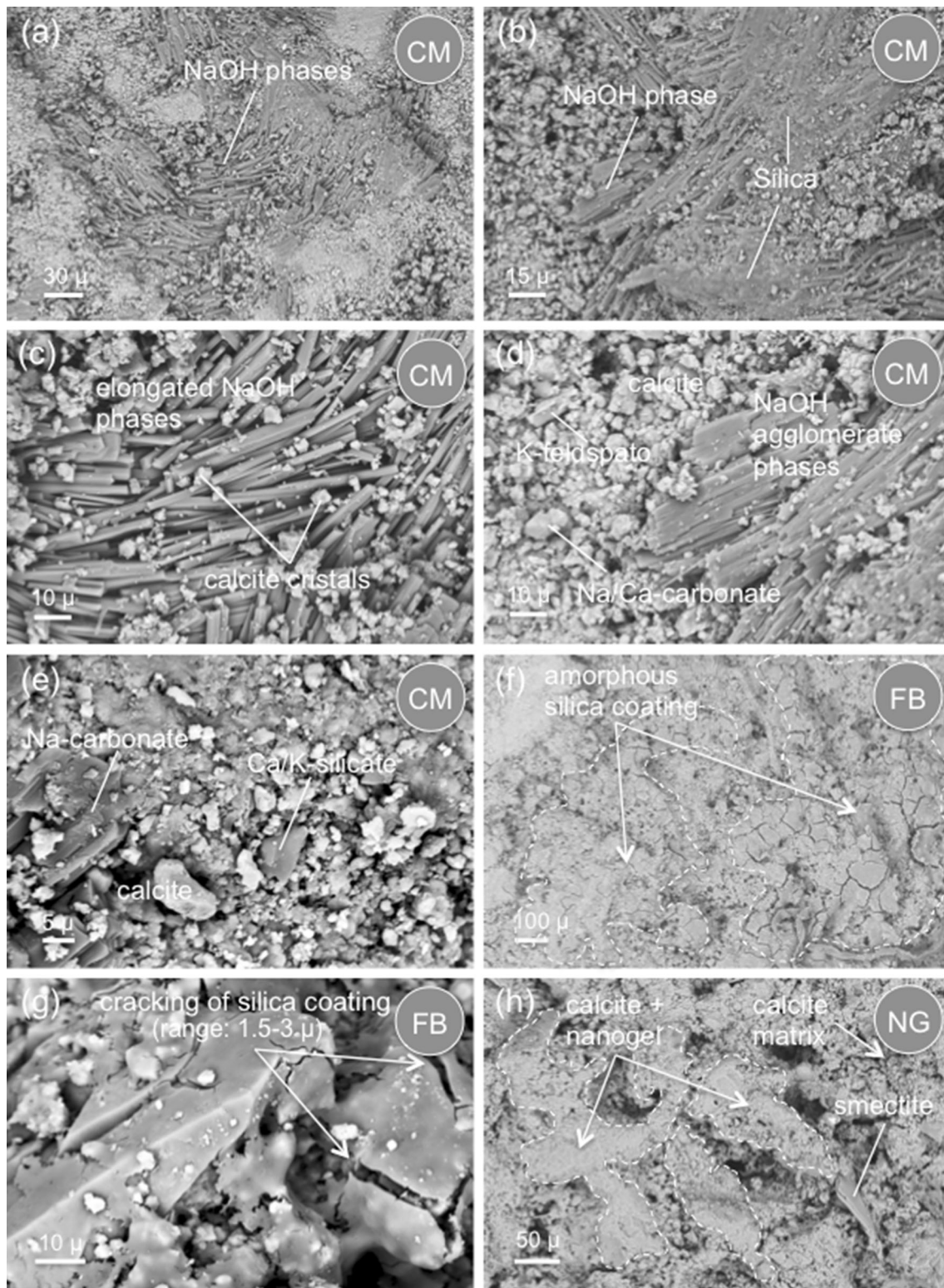
anisotropy of rock, the results show different velocity values as a function on the direction of measurement. In the case with the bedding planes/deposition of *Pietra Cantone* stone perpendicular (according to Z axes), there is a fluctuating velocity, depending on drying time and type of chemical. In the case with parallel planes to measurement direction (according to X and Y), where the pores and crystals (and non-crystalline phases) are more orientated, with the passage of time, at 8 and 15 days, an increase in ultrasonic velocities of the specimens treated with CM and FB is observed (Figs. 9d, 13).

A validation of the consolidation effectiveness was obtained comparing the test results of punching resistance of untreated and consolidated samples. In Table 6 and Fig. 9d, main data are reported: the untreated MSA, MSB and MSC samples have average values of PLT index of 0.50, 0.70 and 1.28 MPa, respectively. The samples which have been treated with the consolidating CM have average higher values than samples which have not been treated with values of 1.13, 1.15 and 1.42 MPa, respectively. The treated with the ethyl silicate hardener FB samples provided in all areas of levy the highest values of PLT index: 1.79, 1.66 and 1.87 MPa, respectively.

The compressive strength (Table 6; Fig. 9d) is an important physical parameter to evaluate the degree of post-treatment structure consolidation, because it is an indicator of compactness and of the possible change of total porosity of material and therefore of the durability too. The compressive strengths of untreated MSA and MSB samples are similar, with average values of 9.5 and 9.2 MPa, respectively, while MSC samples, more porous and altered, show a value of 7.4 MPa. Observing the post-consolidating data, it is noted that the resistances grow considerably in a differentiated way in the two used products: in the case of CM, the increases are of 52 and 39% in the rock types MSA and MSB, and 67% in MSC; in the case of the product FB, the values are of the 143, 91 and 151%, respectively.

In the same way, also the data of ultrasonic velocity, measured in Z axis before and after treatments on the same samples (Table 6; Fig. 9d) where they were performed compressive tests, show a clear increase in compactness in the treated samples due to a decrease in open porosity. Data are differentiated in the two consolidating products. In the case of CM, we have the maximum increase in ultrasonic velocities that passing from 553 (in untreated sample) to 1344 m/s in MSA treated sample, from 652 to 2024 m/s in MSB, and from 919 to 1393 m/s in MSC. In the case of FB, the velocities of the treated samples MSA, MSB and MSC have the following values: 2008, 1196 and 1415 m/s (Table 6).

Even in the case of flexural test, the results indicate an improvement of the strength (Table 6; Fig. 9d). The values of the untreated samples of MSA, MSB and MSC are of



0.7, 0.7 and 0.6 MPa, respectively, while in the treated samples, we have a slight increase in values, although to a lesser extent compared to compressive test data, since understandably the flexural strength is not a very indicative parameter of the consolidation.

However, some considerations must necessarily be made in relation to the application of products and on good performance of the treatment. In fact, the considerable increase in mechanical strength induced by the consolidants with respect to the strength of unaltered stone is

◀**Fig. 12** SEM microphotographs. **a, b, c, d, e** crushed fragment of treated sample with CM consolidant: **a** NaOH agglomerates of surface efflorescence; **b** silica solid phase of consolidant together NaOH agglomerates of surface efflorescence; **c** detail of photo (**a**) with elongated NaOH phases with scattered calcite crystals; **d** detail of photo (**b**) NaOH agglomerate phases and Na/Ca-carbonate fragment with K-feldspar and calcite crystals of muddy matrix; **e** Na-carbonate and Ca/K-silicate fragments and calcite crystals of muddy matrix; **f, g** samples treated with FB consolidant: **f** inhomogeneous distribution of amorphous silica inside the treated stone (see the parts highlighted by white dashed line); **g** detail of photo (**f**) with cracking of silica (with thickness of 1.5–3 μm) over calcite crystals; **h** sample treated with NG nano-gel protective chemical: surface agglomerates of calcite and smectite crystals of muddy matrix with nano-gel (parts highlighted by white dashed line)

considered by some authors as dangerous and not perfectly performing in a conservative treatment, since, in the case of surface application, it produces a crust of material with different physical–mechanical behaviour from the inner material substrate that is not reached by the product. In this research, the consolidation treatments were made with immersion method of specimens (also to determine the maximum amount absorbable of product by stone), so the samples have been almost completely saturated by chemicals. In practical restoration, this is not always possible, then the chemicals must be applied as two or more coats resulting in lower concentration of chemicals within the stone, in order to allow a better adsorption in depth of

stone, until to reach the unaltered stone. In any case, the mechanical strength of treated stone must be similar to the strength of unaltered stone.

For these reasons, the dilution and quantity of consolidating CM and FB that must be used in limestone of monument depend on the depth and degree of decay. The choice of dilution should therefore be made on site, taking the local decay (weathering) conditions into account of the stone to be treated. In the cases of decayed sample, especially on the surface, low concentrations must be used (e.g., 20–40% in CM; <50% in FB) according to two or more coats, as function on physical decay degree of stone. Higher concentration (>50% in CM; >70% in FB) can be used when the limestone shows high decay of all the stones, and it is possible to apply the products through injection to controlled pressure in order to have a high saturation of the porosity and a good and uniform distribution of the consolidating product within the porous matrix of stone.

In regard to some issues related to the application of the consolidant products, SEM analysis on the external surfaces of the treated samples with CM consolidating, besides the Na/K-silicates (Fig. 12b–e) and amorphous solid silica (Fig. 12b), highlights the presence on surface of NaOH agglomerate salts (as efflorescence) with elongated crystals, often according to a curvilinear trend (Fig. 12a, c).

Table 5 Ultrasonic velocity data measured in the three main orthogonal directions X, Y, Z

Sample	X ultrasound (m/s)	Y ultrasound (m/s)	Z ultrasound (m/s)
MSA	802.57	678.47	553
MSA CM	935.73	911.44	613
MSA FB	1672.24	813.01	795
MSB	832.36	747.38	652
MSB CM	1449.28	1303.57	923
MSB FB	1315.79	1020.75	742
MSC	769.60	848.28	919
MSC CM	1871.21	1081.42	901
MSC FB	1326.92	905.91	784
Measure post-consolidating: (at 7 days + 24 h)			
MSA CM	1253.16	1122.73	1031
MSA FB	1984.13	1960.78	1931
MSB CM	1805.05	1373.66	1326
MSB FB	1851.85	1315.51	1185
MSC CM	1907.34	1298.25	1048
MSC FB	1605.86	1024.75	1208
Measure post-consolidating: (at 14 days + 24 h)			
MSA CM	2334.91	1598.71	1344
MSA FB	2358.49	2202.64	2008
MSB CM	2202.64	2138.08	2024
MSB FB	2142.26	1968.00	1196
MSC CM	2129.31	1836.88	1393
MSC FB	2171.81	1468.09	1415

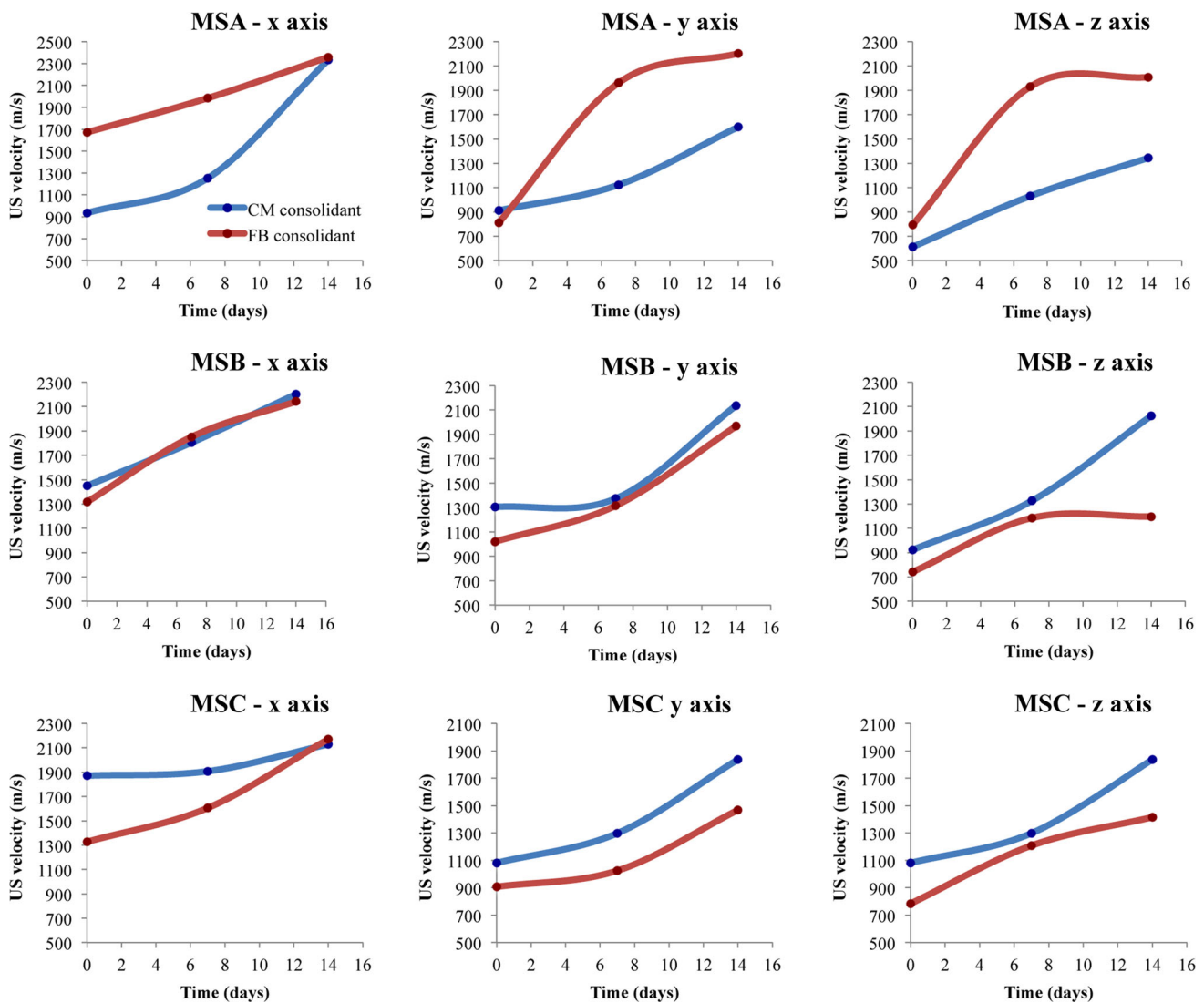


Fig. 13 Ultrasound velocities data in function of time of untreated and treated MSA, MSB, MSC samples of limestone. The graphs show values of not yet consolidated samples MSA, MSB, MSC (velocity value at initial time) and measurement post-consolidation at 8 and 15 days

In the samples treated with FB consolidating (Fig. 12f, g), the cracking on surface of chemical product, with an average thickness of about 2 μm , is observed. Overall, the cracking of the treatment varies from 0.5 to 4 μm . The cracking process may be due also to a rapid evaporation of ethyl alcohol and/or to thermal-differential expansion between the amorphous silica and the crystalline substrate. The spot multispectral chemical analysis shows a silica-based composition.

Conclusions

The results of the physical, mechanical and petrophysical analysis before and after treatment with chemical products on *Pietra Cantone* limestone have allowed to highlight the

effective efficacy of protective and consolidating analysed products.

The protective gel with nanotechnology is a good solution to treat the limestones which are directly exposed to atmosphere, showing the decay that has been by meteoric water (e.g., dissolution of carbonate cement, hydration-dehydration of matrix hygroscopic phases) or, in general, by weathering processes. This product enables to limit the permeability to liquid water phase, as demonstrated by a clear lowering of the open porosity to water, the absorption coefficient and the saturation index, while at the same time, it allows an almost unchanged vapour permeability (transpirability). In some cases, the treatment with nano-gel even facilitates the passage of the vapour phase as evidenced by an increase in the angular coefficient of the straight line graphically representative of the process of permeability.

Table 6 Physical mechanical data of untreated and treated limestone samples: values of Point Load strength index $I_{s(50)}$, flexural strength (Rf), resistance to uniaxial compressive (Rc) and longitudinal wave ultrasound velocities on Z axis

Sample	$I_{s(50)}$ (MPa)	Rf (MPa)	Rc (MPa)	Ultrasound velocity Z axis (m/s)
MSA untreated				
Mean	0.50	0.7	9.48	553.36
SD	0.26	0.14	0.20	
MSA CM				
Mean	1.13	1.1	14.44	1344.09
SD	0.22	0.31	0.46	
MSA FB				
Mean	1.79	1.3	23.08	2008.32
SD	0.12	0.23	0.78	
MSB untreated				
Mean	0.70	0.7	9.21	652.29
SD	0.17	0.18	0.15	
MSB CM				
Mean	1.15	1.2	12.80	2024.29
SD	0.16	0.18	0.43	
MSB FB				
Mean	1.66	0.8	17.55	1208.00
SD	0.20	0.28	0.26	
MSC untreated				
Mean	1.28	0.6	7.40	919.12
SD	0.08	0.1	0.32	
MSC CM				
Mean	1.42	0.8	12.74	1392.76
SD	0.14	0.12	0.22	
MSC FB				
Mean	1.87	1.1	18.57	1415.00
SD	0.36	0.15	0.54	

SD standard deviation

So, according to practice in the stone restoration, the nano-gel can be used as waterproof protective in the preventive conservative treatment of limestones which are characterized by high porosity (>30%) and low cementation degree, in so far as does not allow the passage and absorption of liquid aqueous phases (rain- and condensation-water). In this case, the results showed even a slight increase in the mechanical resistance to work of such protective treatment.

The “Mineral consolidant” CM and ethyl silicate FB treatments of *Pietra Cantone* limestone (with concentrations of 50 and 70%, respectively) lead a clear increase in mechanical strengths as also highlighted by ultrasonic velocity tests. The FB product allows great increases significantly more than the CM, but with a hardening time longer respect to CM. The increase in compressive strength varies from 39 to 67% in the case of the CM product, and from 91 to 151% in the case of FB. As regards to the FB treatment, it has been demonstrated that the presence of illite, or other secondary phases with hydroxyl groups,

eases bonding of the colloidal silica to matrix, forming a compact network able to withstand high mechanical strength to the *Pietra Cantone* limestone. The increase in flexural strength varies from 49 to 63% in CM treatment and from 24 to 102% in the FB.

However, although the considerable increase in mechanical strength induced by the consolidants, in the restore practice, to avoid the formation a surface crust of material with different physical–mechanical behaviour respect to the unaltered material substrate not reached by the product, lower concentrations must be used (<50% in CM and <60% in FB) according to two or more application coats of consolidants.

In the cases where it is possible to use a different application method (e.g., injection to controlled pressure through core drilling), the consolidating CM and FB can be applied with higher concentrations (50–60% in CM; 70–75% in FB), in order to have almost a complete saturation of porosity and a uniform distribution of the consolidating product inside the matrix of stone. This avoids

the formation of compositional heterogeneity that is reflected in time in a damage of the stone. The Indur FB can be applied using an amount of 650 g/m² while CM chemical needs 350 g/m².

In final choice of the type of product, it must also be considered some aspects regarding the unwanted secondary products. Hydrolysis processes of alkaline element and solvent evaporation in the use CM “*Mineral consolidant*” may produce NaOH-efflorescence in some surface portion of stone. Therefore, prior to application of the CM, a careful masonry desalination is recommended with buffered sulfamic acid (H₂NSO₃H) based on the experience gained on the construction site by the Produzioni Freius Chimici company. After their use, it is advisable to apply the lime plaster on building.

As regards to *ethyl silicate* FB, the presence of efflorescence in any samples has not been detected. This chemical is suitable for the consolidation of masonry with stone face-to-view.

The mineralogical-petrographic features (by OM and XRD), chemical SEM–EDS and physical analysis have been necessary and extremely important to verify compatibility between limestone and chemicals, because the different modes of absorption and adhesion of the chemical products to the microstructure of rock affect the restoration efficacy. However, to evaluate the durability of these chemicals and the compatibility in time, further investigations through the accelerated degradation tests in a climatic chamber (in different microenvironmental conditions of humidity, temperature, etc.) and other laboratory tests (salt crystallization, freeze–thaw cycles, UV-light exposure, etc.) must be performed.

Acknowledgements Special thanks to the University of Cagliari for funding of this research, the Superintendence for Archaeological Heritage for the Provinces of Cagliari and Oristano for authorization to sampling of the materials from the monument, the Institute of ‘Scienze dell’Atmosfera e del Clima’ (ISAC)—UOS of Cagliari (C.N.R.) and Research Laboratory for the Protection of Cultural Heritage (Cagliari University) for XRD and SEM analysis, Prof. Guido Ennas of Micro- and Nano-structured Materials Laboratory of Cagliari University for N₂ sorption measurements.

References

- AA.VV. (2002) I silicati nella conservazione, Indagini, esperienze e valutazioni per il consolidamento dei manufatti storici, Atti del congresso internazionale, Villa Gualino, Torino
- AA.VV. (2005) Note illustrative, Carta Geologica d’Italia 1:50.000, Foglio 557 Cagliari. APAT, Servizio Geologico d’Italia, Regione Autonoma della Sardegna
- AA.VV. (2007) Comune di Cagliari, P.U.C. “Urban development plan” of Cagliari, 1997. Scale mapping 1:25.000
- Advokaat EL, Van Hinsbergen DJJ, Maffione M, Langereis CG, Vissers RLM, Cherchi A, Schroeder R, Madani H, Columbu S (2014a) Eocene rotation of Sardinia, and the paleogeography of the western Mediterranean region. *Earth Planet Sci Lett* 401:183–195
- Advokaat EL, Van Hinsbergen DJJ, Maffione M, Langereis CG, Vissers RLM, Cherchi A, Schroeder R, Madani H, Columbu S (2014b) Eocene rotation of Sardinia, and the paleogeography of the western Mediterranean region. Erratum. *Earth Planet Sci Lett* 401:183–195
- Alessandrini G, Bocci A, Bugini R, Emmi D, Peruzzi R, Realini M (1992) Stone materials of Noto (Siracusa) and their decay. In: Proceedings of the 7th international congress on deterioration and conservation of stone (LNEC, Lisbon, 1992). Lisbon, pp 11–20
- Alfano G, Chiancarella C, Cirillo E, Fato I, Martellotta F (2006) Long-term performance of chemical damp-proof courses: twelve years of laboratory testing. *Build Environ* 41(8):1060–1069
- Amoroso G (2002) Trattato di scienza della conservazione dei monumenti. Alinea editrice, Florence
- Antonelli F, Columbu S, Lezzerini M, Miriello D (2014a) Petrographic characterization and provenance determination of the white marbles used in the Roman sculptures of Forum Sempronii (Fossombrone, Marche, Italy). *Appl Phys A Mater Sci Process* 115:1033–1040
- Antonelli F, Columbu S, De Vos Raaijmakers M, Andreoli M (2014b) An archaeometric contribution to the study of ancient millstones from the Mulargia area (Sardinia, Italy) through new analytical data on volcanic raw material and archaeological items from Hellenistic and Roman North Africa. *J Archaeol Sci* 50:243–261
- Arnold A, Zehnder K (1991) Monitoring wall paintings affected by soluble salts. In: Cather S (ed) The conservation of wall paintings, proceedings of a symposium organized by the Courtauld Institute of Art and the Getty Conservation Institute, London, pp 103–135, 13–16 July 1987
- ASTM C 355-64 (1973) Tests for water vapour transmission of thick materials
- ASTM C597 09 (2009) Standard Test Method for pulse velocity through concrete. ASTM International, West Conshohocken
- Atzeni C, Massidda L, Sanna U (1991) Models of dissolution of carbonate materials by acidwaters. *Mater Eng* 2(1):115–126
- Atzeni C, Sanna U, Spanu N (2006) Some mechanisms of microstructure weakening in high-porous calcareous stones. *Mater Struct* 39:525–531
- Barrett EP, Joyner LG, Halenda PP (1951) The determination of pore volume and area distributions in porous substances. I. Computations from nitrogen isotherms. *J Am Chem Soc* 73(1):373–380
- Barroccu G (2010) Urban geology and hydrogeology of the Metropolitan Area of Cagliari. In: Abis E (ed) Il caso di studio dell’Area metropolitana di Cagliari: Pianificazione sostenibile: paesaggio, ambiente, energia. *Future Mac* 09, pp. 116–121, Gangemi editore S.p.A, p 64
- Barroccu G, Crespellani T, Loi A (1981) Caratteristiche geologico-tecniche del sottosuolo dell’area urbana di Cagliari. *Riv Ital Geotec* XV:98–144
- Bertorino G, Franceschelli M, Marchi M, Lugli  C, Columbu S (2002) Petrographic characterisation of polished stone axes from Neolithic Sardinia, archaeological implications. *Per Mineral* 71:87–100
- Bontle M, Nadiye-Tabbiruka MS (2007) Chemical and thermal characterization of a clayey material found near Gaborone Dam. *J Appl Sci Environ Manag* 11(4):77–80
- Brown G (1961) The X-Ray Identification and Crystal Structures of Clay Minerals. Mineralogical Society (Clay Minerals Group), London, p 544
- Camaiti M, Columbu S (2016) Chemical and petrophysical methodological protocol in the consolidation and protection of altered stones in historical monuments. In: Verdiani G (ed) Proceedings of FortMed 2016 international conference, vol 4. Didapress, Firenze, pp 171–178

- Carman PC (1937) Fluid flow through a granular bed. *Trans Inst Chem Eng* 15:150–167
- Carmignani L, Sassi EP (1991) Contribution to the geology of Italy with special regard to the Paleozoic basement Volume dedicated to Tommaso Cocozza. IGCP project, special issue No 276 newsletter, vol. 5, p 215
- Casula G, Cherchi A, Montadert L, Murru M, Sarria E (2001) The Cenozoic graben system of Sardinia (Italy): geodynamic evolution from new seismic and field data. *Mar Pet Geol* 18:863–888
- Che C, Glotch TD, Bish DL, Michalski JR, Xu W (2011) Spectroscopic study of the dehydration and/or dehydroxylation of phyllosilicate and zeolite minerals. *J Geophys Res Planets* 116(E5):1–23
- Cherchi A (1971) Appunti biostratigrafici sul Miocene della Sardegna (Italia). *Mem. BRGM* 78:433–445
- Cherchi A, Tremolieres P (1984) Nouvelles données sur l'évolution structurale au Mésozoïque et au Cénozoïque de la Sardaigne et leurs implications géodynamiques dans le cadre méditerranéen. *C R Acad Sci Paris* 298:889–894
- Chararas B, Cuccuru F, Fais S, Papanikolaou H (2015) Application of non destructive ultrasonic techniques for the analysis of the conservation status of building materials in monumental structures. In: Lollino G et al (eds) *Engineering geology for society and territory*, vol 8. Springer, New York, pp 139–146
- Cocco O, Carboni M, Carcangiu G, Meloni P, Murru A, Persia F, Solla L (2015) Crime Art on the stone: graffiti vandalism on cultural heritage and the anti-graffiti role in its surfaces protection. *Period di Miner* 84(3A):435–452
- Colback PSB, Wiid BL (1965) The influence of moisture content on the compressive strength of rocks. In: *Proceedings of the 3rd symposium Canadian rock mechanics*. Toronto, pp 65–83
- Columbu S (2017) Provenance and alteration of pyroclastic rocks from the Romanesque Churches of Logudoro (north Sardinia, Italy) using a petrographic and geochemical statistical approach. *Appl Phys A Mater Sci Process*. doi:10.1007/s00339-017-0790-z
- Columbu S, Garau AM (2017) Mineralogical, petrographic and chemical analysis of geomaterials used in the mortars of Roman Nora theatre (south Sardinia, Italy). *Ital J Geosci* doi:10.3301/IG.2017.05
- Columbu S, Pirinu A (2016) Use of stone and construction technologies in the medieval and modern fortifications of Cagliari (south-Sardinia, Italy). In: Verdiani G (ed) *Proceedings of FortMed 2016 international conference*, vol 4. Didapress, Firenze, pp 195–202
- Columbu S, Sitzia F (2016) Geochemical and petrophysical characterization of volcanic raw materials with pozzolanic activity used in Roman ancient mortars: some case study. In: Verdiani G (ed) *Proceedings of FortMed 2016 international conference*, vol 4. Didapress, Firenze, pp 203–210
- Columbu S, Verdiani G (2012) From the small elements to the urban scale: an investigation where petrophysical study of materials and architectural shape analysis try to read a masterplan in the Hadrian's Villa, Tivoli (Rome, Italy). In: Börner W, Uhlirz S (eds) *CHNT16 urban archaeology and prospection*. Museen der Stadt - Stadtarchäologie, Wien
- Columbu S, Verdiani G (2014) Digital survey and material analysis strategies for documenting, monitoring and study the romaneseque Churches in Sardinia, Italy. *Lect Notes Comput Sci* 8740:446–453
- Columbu S, Garau AM, Macciotta G, Marchi M, Marini C, Carboni D, Ginesu S, Corazza G (2011) Manuale sui materiali lapidei vulcanici della Sardegna centrale e dei loro principali impieghi nel costruito. Iskra Edizioni, Ghilarza
- Columbu S, Guccini G, Verdiani G (2013) Petro-physical characterization and 3D digital modeling for geometric reconstruction of the Neolithic “domus de janas” of Sedini field (North-Sardinia, Italy). *Adv Comput Sci Int J* 1:70–80
- Columbu S, Antonelli F, Lezzerini M, Miriello D, Adembri B, Blanco A (2014a) Provenance of marbles used in the Heliocaminus Baths of Hadrian's Villa (Tivoli, Italy). *J Archaeol Sci* 49:332–342
- Columbu S, Gioncada A, Lezzerini M, Marchi M (2014b) Hydric dilatation of ignimbritic stones used in the church of Santa Maria di Otti (Oschiri, northern Sardinia, Italy). *Ital J Geosci* 133:149–160
- Columbu S, Marchi M, Martorelli R, Palomba M, Pinna F, Sitzia F, Tanzini L, Virdis A (2015a) Romanesque and Territory. The construction materials of Sardinian Medieval churches: new approaches to the valorisation, conservation and restoration. In: *Proceedings of the 19th international conference on cultural heritage and new technologies, CHNT19*, Museen der Stadt, Stadtarchäologie, Wien, 3–5 Nov 2014
- Columbu S, Sitzia F, Verdiani G (2015b) Contribution of petrophysical analysis and 3D digital survey in the archaeometric investigations of the Emperor Hadrian's Baths (Tivoli, Italy). *Rend Fis Acc Lincei* 26:455–474
- Columbu S, Cruciani G, Fancello D, Franceschelli M, Musumeci G (2015c) Petrophysical properties of a granite-protomylonite-ultramylonite sequence: insight from the Monte Grighini shear zone, central Sardinia, Italy. *Eur J Mineral* 27(4):471–486
- Columbu S, Sitzia F, Ennas G (2016a) The ancient pozzolanic mortars and concretes of Heliocaminus baths in Hadrian's Villa (Tivoli). *Archaeol Anthropol Sci*, Italy). doi:10.1007/s12520-016-0385-1
- Columbu S, Lisci C, Sitzia F (2016b) K/Na-silicate, ethyl-silicate and silane nano-molecular treatments in the restoration of high porous limestone. In: Verdiani G (ed) *Proceedings of FortMed 2016 international conference*, vol 4. Didapress, Firenze, pp 187–194
- Concu G, Fais S (2003) In time analysis of a viscous coupling agent effect in ultrasonic measurements. In: *Proceedings of 3rd international conference on non-destructive testing of the hellenic society for NDT-NDT in antiquity and Nowadays-Skills-Applications- Innovations*, Chania
- Concu G, Valdes M (2007) Correlazione tra velocità ultrasonica e caratteristiche fisico-meccaniche nella calcarenite di Cagliari. In: *Conferenza Nazionale sulle Prove non Distruttive Monitoraggio Diagnostica, 12° Congresso Nazionale dell'AIPnD*, Milano
- Concu G, De Nicolo B, Mistretta F (2003a) Comparative evaluation of two non-destructive acoustic techniques applied in limestone masonry diagnosis. In: *Proceedings of 33rd international conference and exhibition defectoscopy*, Ostrava. ISBN 80-214- 2499-0
- Concu G, De Nicolo B, Mistretta F, Valdés M (2003b) NDT ultrasonic method for ancient stone masonry diagnosis in Cagliari (Italy). In: *Proceedings of structural faults and repair—2003*, London. ISBN 0-947644-52-0
- Concu G, De Nicolo B, Valdes M (2014) Prediction of building limestone physical and mechanical properties by means of ultrasonic P-wave velocity. *Sci World J* 2014:1–8. doi:10.1155/2014/508073
- Coroneo R, Columbu S (2010) Sant'Antioco di Bisarcio (Ozieri): la cattedrale romanica e i materiali costruttivi. *Archeoarte* 1:145–173
- Croveri P, Dei L, Giorgi R, Salvadori B (2004) Consolidation of globigerina limestone (Malta) by means of inorganic treatments: preliminary results. In: *Proceedings of the 10th international congress on deterioration and conservation of stone*, Stockholm
- Cuccuru F, Fais S, Ligas P (2014) Dynamic elastic characterization of carbonate rocks used as building materials in the historical city

- centre of Cagliari (Italy). *Q J Eng Geol Hydrogeol* 47(3):259–266
- Diana G, Fais S (2011) IR thermography and ultrasonic investigations in the Cultural Heritage field. In: Museen der Stadt Wien-Stadtarchäologie (ed) Proceedings of the workshop 15 international conference on cultural heritage and new technologies. Museen der Stadt Wien-Stadtarchäologie, Vienna, pp 643–648
- Dunham RJ (1962) Classification of carbonate rocks according to depositional texture in W.E. Ham, Classification of carbonate rocks. *Am Assoc Pet Geol Mem* 1:108–121
- Escalante MR, Valenza J, Scherer GVW (2000) Compatible consolidant from particle-modified gels. In: Proceedings of the 9th international congress on deterioration and conservation of stone, Venice
- Fais S, Cuccuru F, Ligas P, Casula G, Bianchi MG (2015) Integrate ultrasonic, laser scanning and petrographical characterization of carbonate building materials on an architectural structure of historic building. *Bull Eng Geol Environ* 76(1):71–84
- Folk RL (1959) Practical petrographic classification of limestones. *Am Assoc Pet Geol Bull* 43:1–38
- Francis A, Dullien L (1975) New network permeability model of porous media. *AIChE J* 21:299–307
- Franzoni E, Pigino B, Pistolesi C (2013) Ethyl silicate for surface protection of concrete: performance in comparison with other inorganic surface treatments. *Cem Concr Compos* 44:69–76
- Gandolfi R, Porcu A (1967) Contributo alla conoscenza delle microfaccie mioceniche delle colline di Cagliari (Sardegna). *Riv It Paleont* 78(1):313–348
- Giamello M, Columbu S, Droghini F, Scala A, Terrosi A (2016) Ancient surface treatments of the historical architecture: methodological data comparison from different study cases. In: Verdiani G (ed) Proceedings of FortMed 2016 international conference, vol 4. Didapress, Firenze, pp 235–242
- Goins ES, Wheeler GS, Wypshski MT (1996) Proceedings of the 8th international congress on deterioration and conservation of stone, vol. III, Berlin, pp 1255–1264
- Gray SE (2000) A study of composite action in material after treatment. University of Pennsylvania, Philadelphia
- Guerrero MA, Vazquez MA, Galan E, Zezza F (1990) The physical-mechanical properties and ultrasonic data as criteria for evaluation of calcareous stone decay. In: Zezza F (ed) Proceedings of the 1st international symposium the conservation of monuments in the Mediterranean basin. Grafo Edizioni, Brescia, pp 309–312
- ISRM, International Society for Rock Mechanics (1972) Suggest method for determining the point load strength index. ISRM (Lisbon, Portugal). Committee on Field Tests. Document n.1, pp 8–12
- ISRM, International Society For Rock Mechanics (1985) Suggest method for determining the point load strength ISRM Commission for testing methods, working group on revision of the point load test methods. *Int J Rock Mech Min Sci Geomech Abstr* 22:51–60
- Larry D et al (1996) Aqueous dispersible oil and water repellent silane masonry penetrants. Minnesota mining and manufacturing company, Minnesota, p 2
- Lezzerini M, Antonelli F, Columbu S, Gadducci R, Marradi A, Miriello D, Parodi L, Secchiari L, Lazzeri A (2016) The documentation and conservation of the cultural heritage: 3D laser scanning and GIS techniques for thematic mapping of the stonework of the façade of St. Nicholas Church (Pisa, Italy). *Int J Archit Herit Conserv Anal Restor* 10(1):9–19
- Lopez-Arce P, Doehne E, Greenshields J, Benavente D, Young D (2009) Treatment of rising damp and salt decay: the historic masonry buildings of Adelaide, South Australia. *Mater Struct* 42(6):827–848
- Lovisato D (1901) Le calcaire jaunatre de Pirri del Lamarmora e i calcari di Cagliari come pietra di costruzione. Tipo-Litografia Commerciale Ed., Cagliari, p 82
- Macciotta G, Bertorino G, Caredda A, Columbu S, Coroneo R, Franceschelli M, Marchi M, Rescic S (2001) The S. Antioco of Bisarcio Basilica (NE Sardinia, Italy): water-rock interaction in ignimbrite monument decay. In: Cidu R (ed) Water-Rock Interaction 2001. Swets & Zeitlinger, Lisse, pp 415–418
- Mameli PL (2012) Problemi di consolidamento di matrici lapidee di differente microstruttura esposte a sollecitazioni ambientali e microclimatiche di varia origine. Dissertation thesis, Alma Mater Studiorum, Università di Bologna. Dottorato di ricerca in Ingegneria dei materiali. doi:10.6092/unibo/amsdottorato/4824
- Melis S, Columbu S (2000) Matériaux de construction en époque romaine et avec les ancennescarrières: l'exemple du theatre de Nora (Sardaigne SO, Italie). In: Lorenz J, Tardy D, Coulon G (eds) Proceedings of International Congress “La pierre dans la ville antique et médiéval - Analyse méthodologie et apports”, Mémoire 3 du Musée d'Argentomagus, “18° supplément à la Revue Archéologique du Centre de la France”, Argentoun sur Creuse, pp 103–117
- Miriello D, Antonelli F, Apollaro C, Bloise A, Bruno N, Catalano E, Columbu S, Crisci GM, De Luca R, Lezzerini M, Mancuso S, La Marca A (2015) A petro-chemical study of ancient mortars from the archaeological site of Kyme (Turkey). *Per Mineral* 84:497–517
- NORMAL 21/85 (1985) Permeabilità al vapor d'acqua. NORMAL Commission Recommendation
- Ozturk I (1992) Alkoxysilanes Consolidation of Stone and Earthen Building Materials, Master's thesis, University of Pennsylvania
- Pala A, Siriu E (1997) Carta Idrogeologica di Cagliari in scala 1:10.000. Dipartimento di Scienze della Terra, Università degli Studi di Cagliari
- Pecorini G, Pomesano Cherchi A (1969) Geological and biostratigraphic researches on Southern Campidano (Sardegna). *Mem Soc Geol Ital* 8:421–451
- Plenderleith HJ, Werner AEA (1973) The Conservation of Antiquities and Works of Art. *Stud Conserv* 18(4):189–194
- Price CA (1996) Stone conservation, an overview of current research. The Getty Conservation Institute, Santa Monica
- Rodolico F (1953) Stones of the Italian cities. (Le Monnier, Firenze). Only available in Italian
- Rodriguez Navarro C, Guidetti V, Chiavarini M, Sebastian Pardo E (1996) Studies on the protective-reaggregating fluorurethanes on lithotypes with different porosity and pore-size distribution. In: Proceedings of the 1995 LCP Cong. On Preservation and Restoration of Cultural Heritage, Montreux 1995, pp 711–721
- Salazar Hernández C, Puy Alquiza MJ, Salgado P, Cervantes J (2010) TEOS-colloidal silica-PDMS-OH hybrid formulation used for stone consolidation. *J Appl Organomet Chem* 24:481–488
- Sing KSW, Everet DH, Haul RAW, Moscou L, Pierotti RA, Rouquerol J, Siemieniewska T (1985) Reporting physisorption data for gas/solid systems with special reference to the determination of surface area and porosity. Recommendations 1984. *IUPAC. Pure Appl Chem* 57(4):603–619
- Spadola G (2005) Il restauro con prodotti chimici. I prodotti, il cantiere, le tecniche, le misure di sicurezza
- Sponchia G (2011) Studio di nanoparticelle di silice mesoporose e loro utilizzo come supporto per la sintesi di particelle di dimensione controllata
- UNI EN 12372 (2001) Natural stone test methods. Determination of flexural strength under concentrated load
- UNI EN 12504-4 (2005) Testing concrete. Part 4: Determination of pulse ultrasonic velocity
- UNI EN 1926 (2007) Natural stone test methods. Determination of uniaxial compressive strength
- Vannucci S, Alessandrini G, Cassar J, Tampone G, Vannucci ML (1994) Prehistoric megalithic temples of the maltese arcipelago: causes and mode of deterioration of globigerina limestone. In:

- Fassina V, Ott H, Zezza F (eds) Proceedings of the 3rd international symposium the conservation of monuments in the mediterranean basin, Venezia. Soprintendenza ai Beni Artistici e Storici di Venezia, Venezia, pp 555–565
- Vardabasso S (1962) Questioni paleogeografiche relative al Terziario antico della Sardegna. *Mem Soc Geol Ital* 3:655–673
- Verdiani G, Columbu S (2010) E. Stone, an archive for the Sardinia monumental witnesses. *Lect Notes Comput Sci* 6436:356–372
- Walton KS, Snurr RQ (2007) Applicability of the BET method for determining surface areas of microporous metal-organic frameworks. *J Am Chem Soc* 129(27):8552–8556
- Wheeler G (2005) Alkoxysilane and stone conservation. Getty publication, Los Angeles, pp 83–100
- Zeza U, Veniale F, Zezza F, Moggi G (1990) Effects of water saturation on the pietra leccese mechanical weakening. In: Zezza F (ed) Proceedings of the 1st international symposium the conservation of monuments in the Mediterranean Basin. Grafo Edizioni, Brescia, pp 263–269
- Zinsmeister L, Dautriat J, Bornert M, Gland N, Dimanov A, Raphanel J (2012) Mechanical behavior of an altered reservoir limestone: multi-scale and core analysis approach. In: Proceedings of international symposium 2012, Society of Core Analysts. Aberdeen, SCA2012-10, pp 1–12